ERDC/GSL TR-12-16

Geotechnical and Structures Laboratory

US Army Corps
of Engineers®
Engineer Research and
Development Center

ERDC
INNOVATIVE SOLUTIONS
for a safer, better world

Reformulation of the CBR Procedure

Report II: Design, Construction, and Behavior Under Traffic of the Pavement Test Sections

Carlos R. Gonzalez, Walter R. Barker,
and Alessandra Bianchini

December 2013

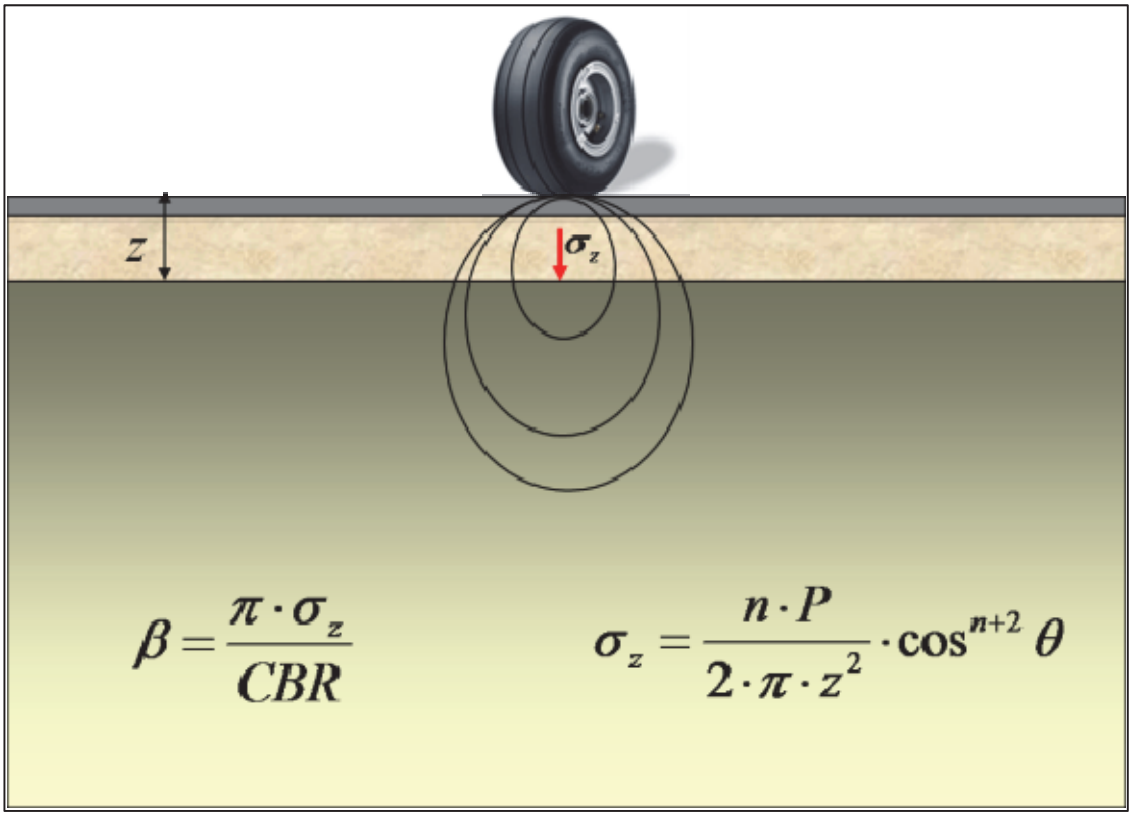

The US Army Engineer Research and Development Center (ERDC) solves the nation's toughest engineering and environmental challenges. ERDC develops innovative solutions in civil and military engineering, geospatial sciences, water resources, and environmental sciences for the Army, the Department of Defense, civilian agencies, and our nation's public good. Find out more at www.erdc.usace.army.mil.

To search for other technical reports published by ERDC, visit the ERDC online library at http://acwc.sdp.sirsi.net/client/default.

ERDC/GSL TR-12-16
December 2013

Reformulation of the CBR Procedure

Report II: Design, Construction, and Behavior Under Traffic of the Pavement Test Sections

Carlos R. Gonzalez, Walter R. Barker, and Alessandra Bianchini

Geotechnical and Structures Laboratory
US Army Engineer Research and Development Center
3909 Halls Ferry Road
Vicksburg, MS 39180-6199

Report 2 of a series

Prepared for US Army Corps of Engineers
Washington, DC 20314-1000

Abstract

The California Bearing Ratio (CBR) procedure has been the principal method used for design of flexible pavements for both military roads and airfields since its development in the 1940s. In recent years, as the use of analytical models, such as the layered elastic and finite element models, became accepted for pavement design, the CBR design procedure was criticized as being empirical, overly simplistic, and outdated. A major criticism of the procedure was the use of a correction factor (Alpha factor) as a thickness adjustment for traffic volume. The objectives of this research were to reformulate the CBR-Alpha procedure so that design would be based on a more mechanistic methodology and to develop performance criteria for use with the reformulation. With these purposes in mind, this report details the developmental steps of the reformulation, starting with the original CBR-Alpha procedure and ending with a new procedure based on Fröhlich's theory for stress distribution. The reformulation was verified through review of historical test data and full-scale traffic tests and analyses of an actual airfield pavement failure. The reformulation of the procedure resulted in the elimination of both the equivalent single-wheel load concept and the Alpha factor.

Contents

Figures and Tables

Figures

Tables

Preface

The US Air Force Civil Engineer Center (AFCEC) tasked the US Army Engineer Research and Development Center (ERDC), Geotechnical and Structures Laboratory (GSL), to investigate the fundamentals of the California Bearing Ratio (CBR) procedure, which has been the principal method used for design of flexible pavements for both military roads and airfields since its development in the 1940s. The objectives were to reformulate the CBR-Alpha procedure so that designs would be based on a more mechanistic methodology and to develop performance criteria for use with the reformulation.

The research was conducted by personnel in the Airfields and Pavements Branch (APB), Engineering Systems and Materials Division (ESMD), GSL. The research team consisted of Dr. Walter R. Barker, SOL Engineering Service, LLC, and Carlos R. Gonzalez, APB. This report was prepared by Gonzalez, Barker, and Dr. Alessandra Bianchini, APB.

During this project, Dr. Gary L. Anderton was Chief, APB; Dr. Larry N. Lynch was Chief, ESMD; Dr. William P. Grogan was Deputy Director, GSL; and Dr. David W. Pittman was Director, GSL.

At the time of publication, COL Jeffrey Eckstein was Commander and Executive Director of ERDC. Dr. Jeffery P. Holland was Director.

Unit Conversion Factors

Multiply	By	To Obtain
cubic feet	0.02831685	cubic meters
cubic inches	1.6387064 E-05	cubic meters
cubic yards	0.7645549	cubic meters
degrees Fahrenheit	(F-32)/1.8	degrees Celsius
feet	0.3048	meters
foot-pounds force	1.355818	joules
inches	0.0254	meters
inch-pounds (force)	0.1129848	newton meters
microinches	0.0254	micrometers
microns	1.0 E-06	meters
miles (US statute)	1,609.347	meters
miles per hour	0.44704	meters per second
mils	0.0254	millimeters
pounds (force)	4.448222	newtons
pounds (force) per foot	14.59390	newtons per meter
pounds (force) per inch	175.1268	newtons per meter
pounds (force) per square foot	47.88026	pascals
pounds (force) per square inch	6.894757	kilopascals
pounds (mass)	0.45359237	kilograms
pounds (mass) per cubic foot	16.01846	kilograms per cubic meter
pounds (mass) per cubic inch	2.757990 E+04	kilograms per cubic meter
pounds (mass) per square foot	4.882428	kilograms per square meter
pounds (mass) per square yard	0.542492	kilograms per square meter
square feet	0.09290304	square meters
square inches	6.4516 E-04	square meters

1 Introduction

The California Bearing Ratio (CBR) procedure has been the principal method used for design of flexible pavements for both military roads and airfields since its development in the 1940s. As the use of analytical models, such as the layered elastic and finite element models, became accepted for pavement design, the CBR design procedure was criticized as being empirical, overly simplistic, and outdated. The need for this study originated as a response to the ongoing criticism of the CBR procedure as it was originally formulated in the 1940s. The first phase of the study was a reformulation of the analytical model for stress distribution in a pavement system. The second phase included the performance criteria development using the newly defined analytical model with existing performance data. The third phase of the study was to validate the performance criteria with additional data not employed in the second phase. The validation phase required the construction of a full-scale test section for the purpose of adding new data to the pavement performance database. The research findings that resulted in the development of the CBR-Beta design procedure for flexible pavements are documented in Gonzalez et al. (2012).

This report presents a summary of the full-scale test section design, construction, and performance that supported the reformulation of the original CBR procedure.

Background

The CBR procedure was originally developed in the 1940s for the design of flexible pavements to support the new heavy bombers. The original airfield design curves were an extrapolation of the empirically-developed California pavement design curves for highway pavements.

In 1955, the US Army Corps of Engineers proposed the CBR equation as the basis for a flexible airfield pavement design procedure (Middlebrooks, 1950). With the development of heavy multi-wheel aircraft, such as the C-5A and B-747, a thickness adjustment factor (α-factor) was introduced into the CBR equation to account for the effects of traffic repetitions and multi-wheel tire groups (WES, 1971). The α-factor depends on the number of passes over the pavement and the number of wheels on the main landing gear; this information was employed to calculate the equivalent

single-wheel load (ESWL). The α-factor is determined in relation to the number of passes and selecting the curve representative of the number of wheels used for ESWL computation.

The CBR design procedure gained world-wide acceptance as a procedure for airport pavement design and was adopted as the basis for computation of the Aircraft Classification Number (ACN). The 1983 edition of the International Civil Aviation Organization (ICAO) *Aerodrome Design Manual*, which is currently in use, prescribed the CBR procedure as the basis for computing the ACN for civilian aircraft. The ACN is a number of great importance to the aircraft industry because it is instrumental in determining which aircraft individual airports are able to accept for operations.

Criticisms of the CBR design procedure arose from the Information and Technology Platform for Transport, Infrastructure and Public Space (CROW) (2004). The CROW report contained the following statement: "It is now widely recognized that the US Army Corps of Engineers' CBR method cannot adequately compute or predict pavement damage caused by new large aircraft." Specifically, the CBR procedure came under scrutiny with respect to pavement design and ACN evaluation for multi-wheel aircraft. A critical element and the center of the controversy in the ICAO procedure for computing the ACN is the α-factor. In September 2006, the Aerodrome Operations and ICAO Services Working Group (AOSWG) proposed in Discussion Paper No. 21 (DP21) the reformulation of the α-factor at 10,000 coverages for 4- and 6-wheel gears for use in calculating the ACN of airplanes operating on flexible pavements. The α-factor was, in fact, deemed to be inadequate in representing multi-wheel aircraft scenarios.

As a result of the controversy concerning the α-factor, the US Army Engineer Research and Development Center (ERDC) was tasked by the AFCEC to investigate the design issue and to reformulate the CBR procedure. In addition to reviewing the history that led to the definition of the original CBR procedure, the design procedure was analytically reformulated and validated using performance data generated by the construction of a full-scale testing section that was trafficked under different aircraft loads.

Objective and scope

The primary objective of this research was to reformulate the CBR-Alpha procedure to be a more robust mechanistic methodology, independent of the α-factor. Chapter 2 contains the details of the design of the flexible pavement test sections. Chapter 3 discusses the section's construction phase and the laboratory and field measurements for assuring construction quality. Chapter 4 describes the instrumentation installed in each section item. Chapter 5 explains the characteristics of the testing and traffic pattern. Chapter 6 describes testing and the behavior of the section under traffic, and Chapter 7 contains a summary of the findings and recommendations.

2 Test Section Design

General

The test section was constructed for the purpose of validating the CBR-Beta design procedure. The test section consisted of three traffic lanes; each lane was divided into four pavement items with different layer characteristics. Figure 1 shows a profile view of the pavement item layer characteristics.

The wheel loads that were selected for traffic testing included the F-15E tire, the C-17 dual tire, and the C-17 single tire. The tire pressures were of 325 psi and 142 psi for the F-15E and C-17 tires, respectively. These load conditions were selected to evaluate the pavements' structural behavior when subjected to aircraft loads typically included in the Air Force medium to modified-heavy design traffic patterns.

The test section thicknesses above the subgrade varied from 17 in. to 32 in. The asphalt surface and the base layer of crushed limestone had a constant thickness of 3 in. and 6 in., respectively. The subbase thicknesses varied from 8 in. to 23 in. The reasons for maintaining constant asphalt surface and base layer thicknesses were twofold. First, these thicknesses maintained compatibility with the full-scale testing utilized for the multi-wheel heavy gear load (MWHGL) study in which the asphalt surface and the base layer had the thicknesses of 3 in. and 6 in., respectively, for each pavement section (Ledbetter et al. 1971). Second, since the purpose of the test section was to validate the CBR-Beta procedure, which is concerned primarily with the determination of the thickness of the subbase for given subgrade strengths, it was necessary to eliminate asphalt and base thicknesses as variables. The subbase material was sandy gravel with a design CBR of 30%; the subgrade design CBR was 4% for the thicker sections and 10% and 15% for the remaining sections. Figure 1 shows the section construction details.

The coverage levels shown in Figure 1, and therefore the section thicknesses, were initially chosen to fill the gaps (represented by blue ovals in Figure 2) in terms of failure points in the Beta-coverages curve (Figure 2). Figure 1 shows the predicted coverages to failure computed with the CBR-Alpha (in red) and CBR-Beta (in blue) procedures, respectively.

Figure 1. Test section design details.

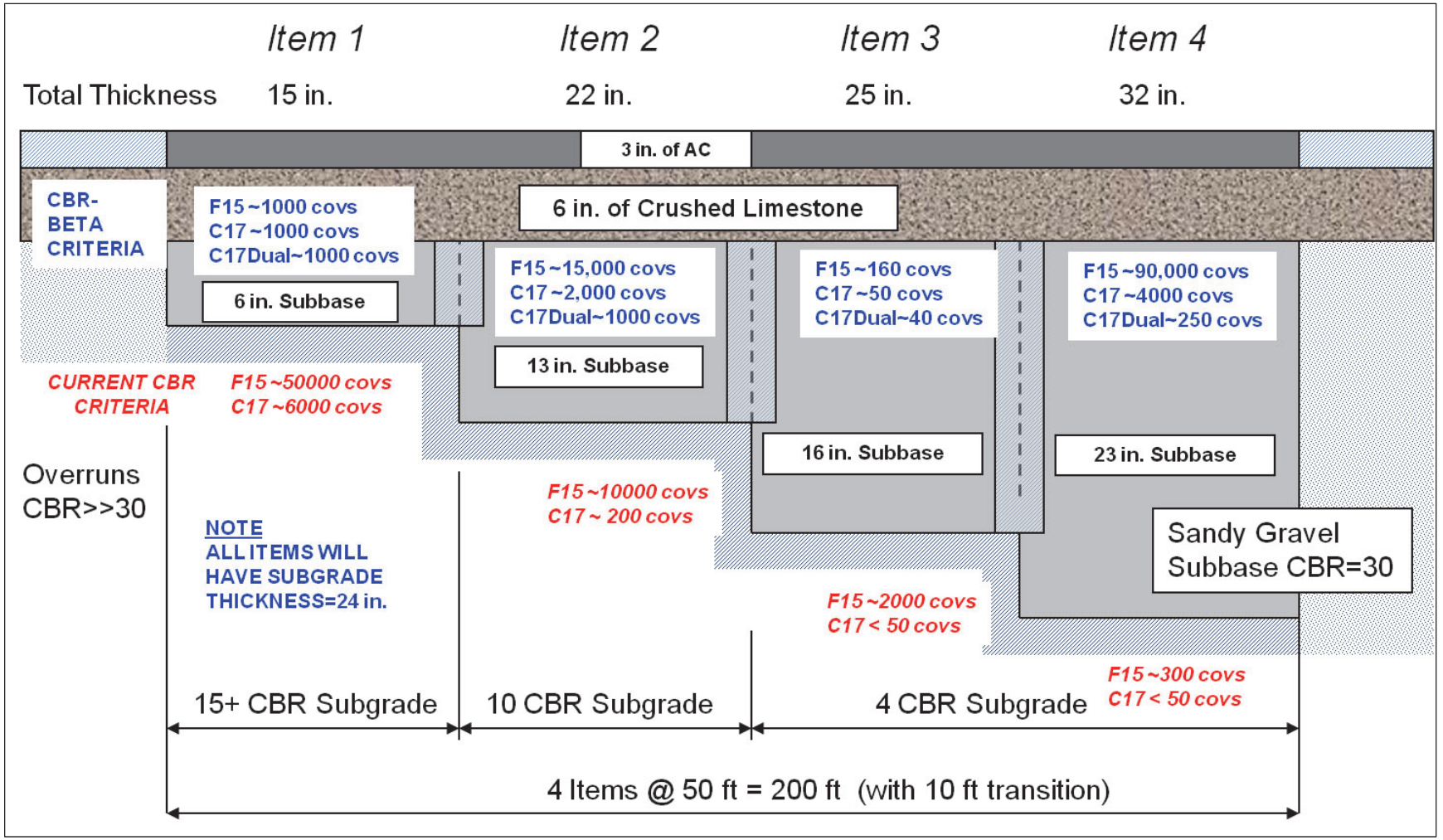

Figure 2. Beta-coverages curve and pavement failure data.

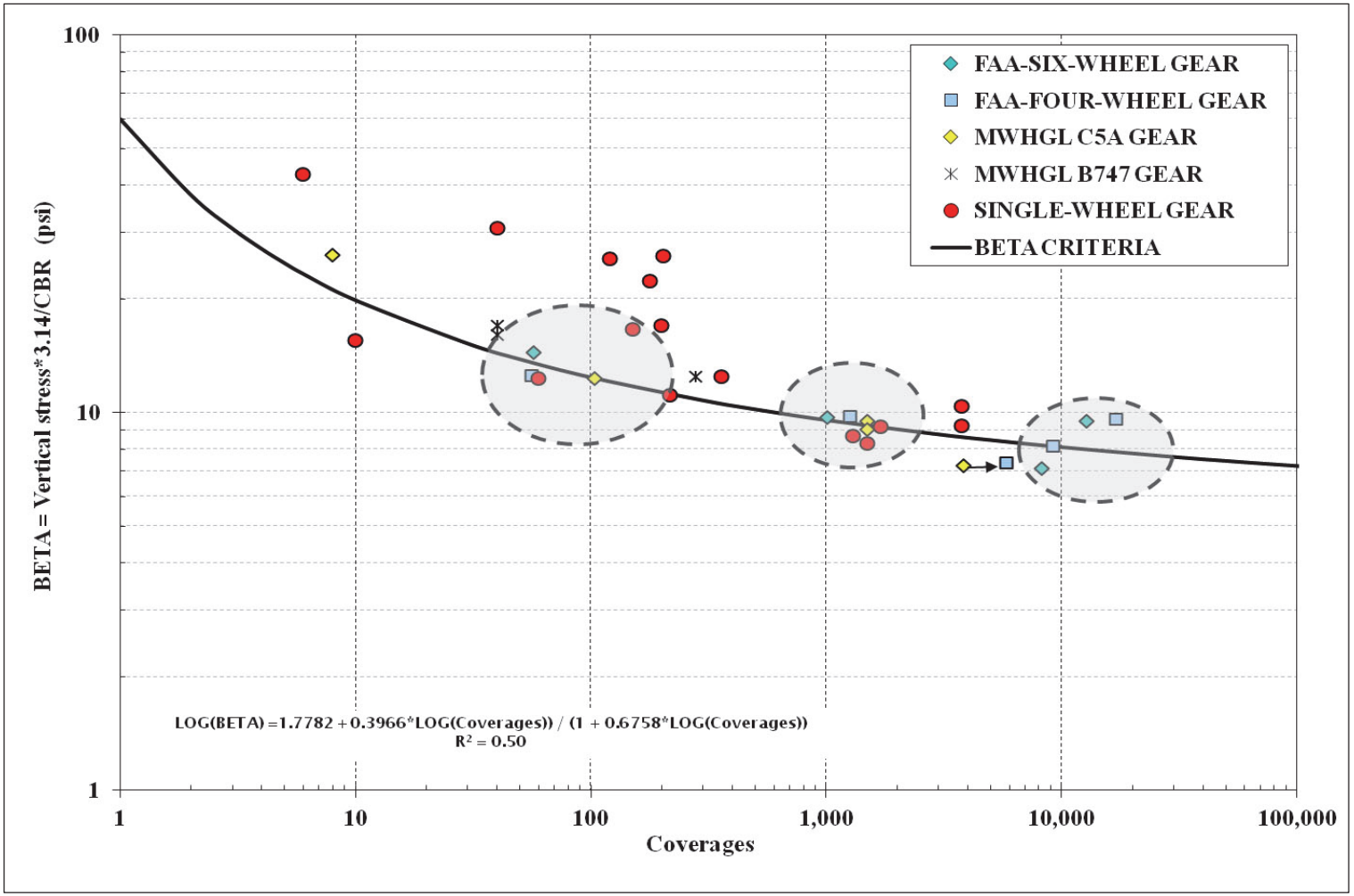

Test site

The full-scale test section was located inside Hangar 4 (Airfields and Pavements Branch testing facility) at the US Army Engineer Research and Development Center, Vicksburg, Mississippi. The facility was covered and protected from rainfall but was not temperature controlled. Figure 3(a) is a view from the south end of the Hangar 4 looking to the north; Figure 3(b) is an aerial view of Hangar 4. The test section was located in the eastern one-half and northern two-thirds of the covered structure.

Figure 3. Testing facility and test sections: (a) south end of Hangar 4and (b) aerial view of Hangar 4.

(a)

(b)

The in situ soil was a lean clay (loess) deposit, and the depth to the groundwater table was approximately 6 ft.

Layout

The test section was 200 ft long and 40 ft wide with paved areas at each end of the section. The test section was divided transversely into four longitudinal test items differentiated by the thickness of the subbase and strength of the subgrade. The test items were 40 ft long and were separated by a 10-ft transition zone. The length of the test section was divided longitudinally into three traffic lanes: Lanes 1 and 3 were for single-wheel traffic, and Lane 2 was for dual-wheel traffic. The traffic lane widths were 5 ft, 10 ft, and 5 ft for the F-15E single-wheel gear (325 psi), C-17 dual-wheel gear (142 psi), and C-17 single-wheel gear (142 psi), respectively. The 5 ft of pavement at each end of the test items was considered as a transition zone

between items and was not considered in the analysis. Figure 4 illustrates the as-constructed cross-section layouts and transition zones between test items. Figure 5 depicts the typical dimensions and type of traffic applied to each item.

Pavement elements

Subgrade

All test items were constructed over a compacted high-plasticity clay (Vicksburg Buckshot Clay) material. The material was extracted from a borrow pit located about 10 miles south of Vicksburg in the floodplain of the Mississippi River. The soil had a Liquid Limit (LL) of 79 and Plasticity Index (PI) of 51, and was classified as high-plasticity clay (CH). The soil's specific gravity was 2.74. The soil gradation curve is contained in Figure 6. The results from laboratory compaction, according to modified Proctor ASTM D1557, are summarized in Figure 7, which shows the clay moisture-density curve.

The design subgrade CBR values selected for the test section construction were 4%, 10%, and 15%. The high plasticity clay moisture content required to achieve these CBR values was determined from moisture content versus CBR relationship (Figure 8) developed at ERDC from historical field and laboratory test data. After placement of the subgrade material, undisturbed samples were obtained to conduct laboratory triaxial compression testing.

Figure 4. Cross-section profiles (as constructed).

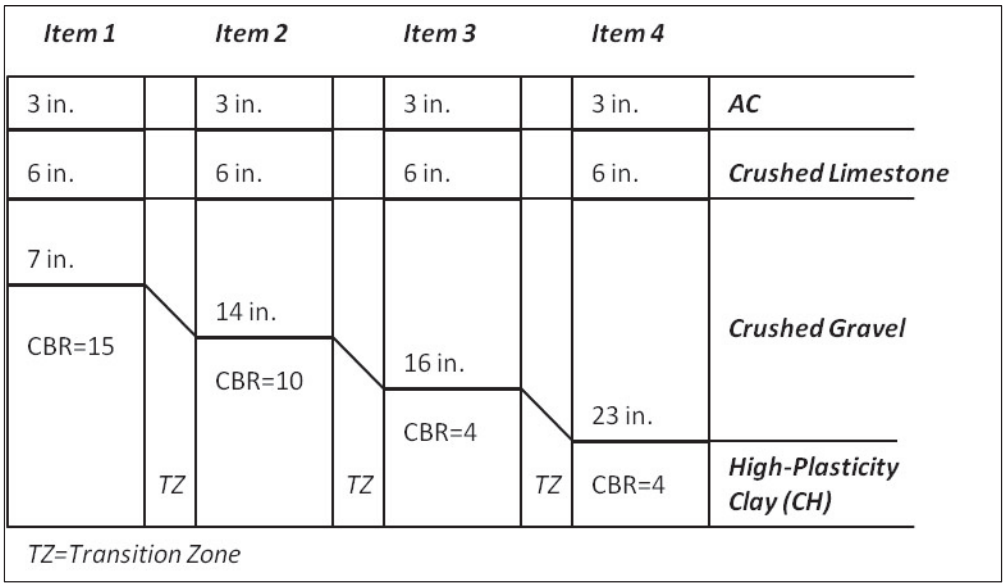

Figure 5. Section layout and traffic lanes.

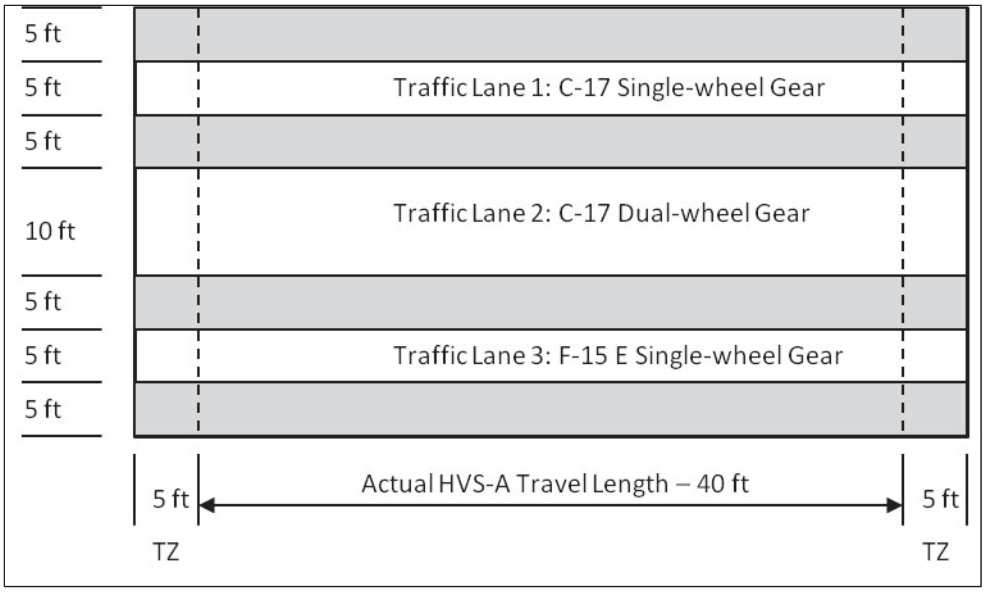

Figure 6. Subgrade (CH) grain-size distribution.

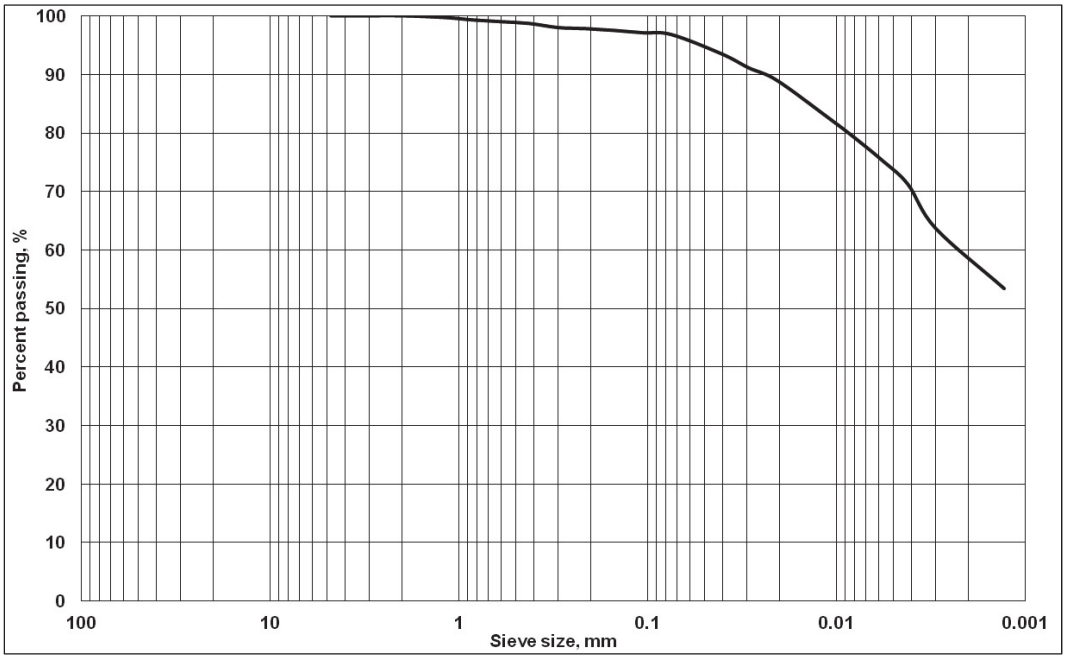

Figure 7. Subgrade moisture-density curve.

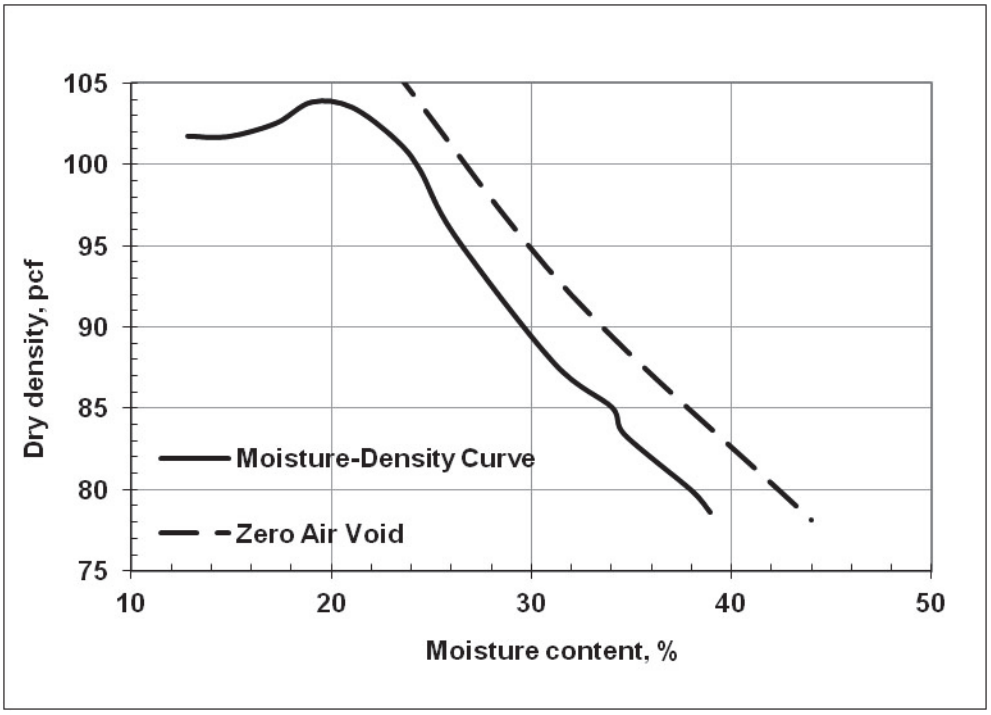

Figure 8. Subgrade CBR-moisture content curve and CBR field test results.

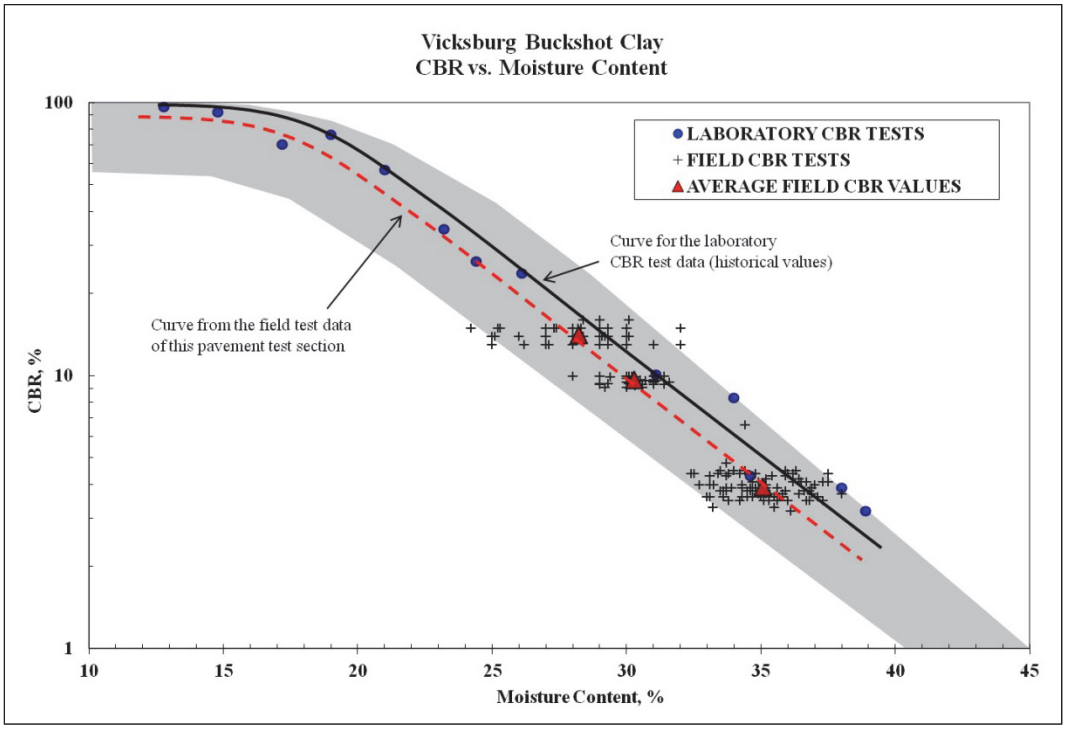

The triaxial tests were drained and had a confining pressure of 15 psi. Laboratory CBR tests were also executed based on the procedure ASTM D1883-07e2; the data are contained in Figure 9, which shows the relationships between moisture content and CBR and failure stress. Figure 10 summarizes the deviatoric stress-strain data from the triaxial tests on the subgrade material characterized by CBR values of 4, 10, and 15 with respective moisture contents of 34%, 30%, and 27%. Figure 11 shows the Mohr's circles from the triaxial test results. Table 1 summarizes strength material properties for each CBR value. The ultimate stress difference was computed using the hyperbolic soil model by Kondner (1963), represented in Equation 1. The failure stress difference was determined from laboratory test results from the test specimens.

Figure 9. Relationships between subgrade material moisture content, CBR, and failure stress.

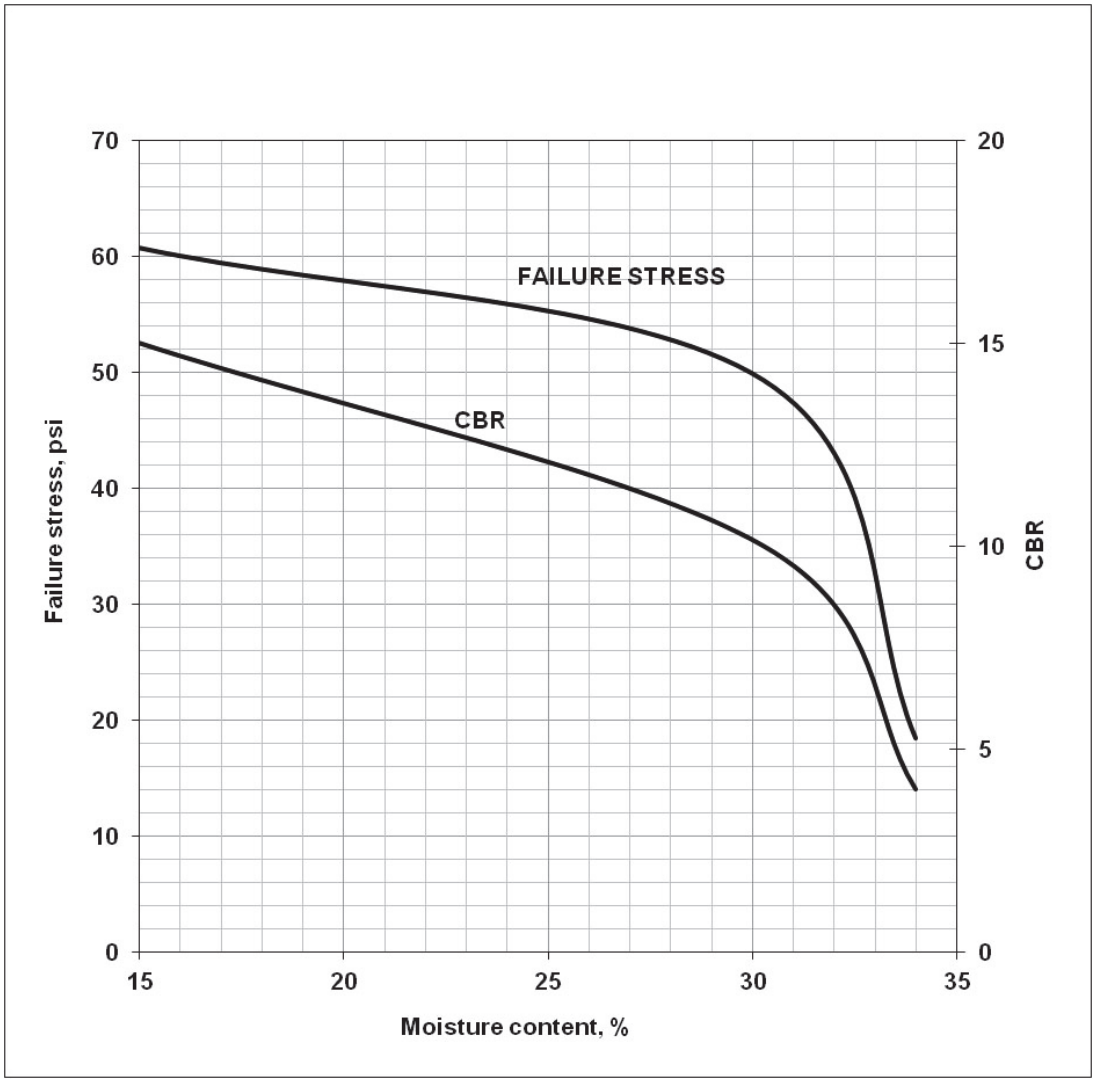

Figure 10. Stress-strain data from confined, drained triaxial compression tests on the subgrade soil.

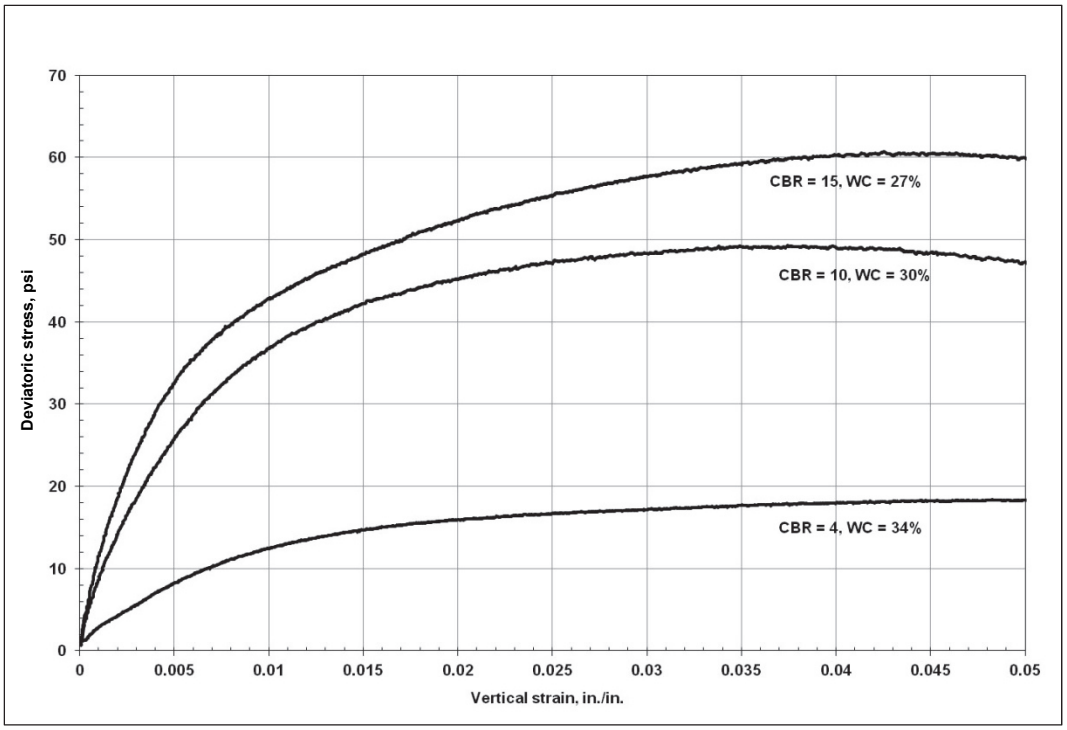

Figure 11. Subgrade material Mohr circles at different CBR values.

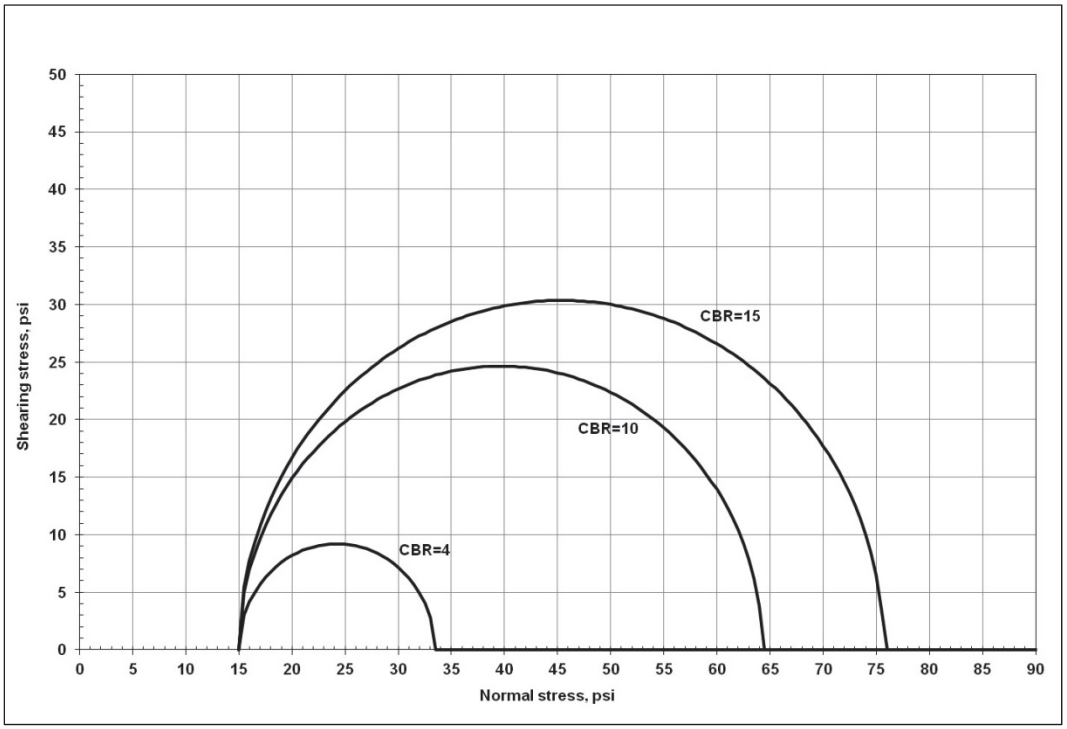

Table 1. Subgrade material characteristics.

CBR	$(\sigma_1-\sigma_3)_{ult}$, psi	$(\sigma_1-\sigma_3)_f$, psi	c, psi	Φ, °	w, %
4	21.2	18.4	9.2	0	34
10	55.1	49.3	25.7	0	30
15	68.9	60.7	30.4	0	27

$$(\sigma_1 - \sigma_3) = \frac{\varepsilon}{\frac{1}{E_i} + \frac{\varepsilon}{(\sigma_1 - \sigma_3)_{ult}}} \quad (1)$$

where:

$(\sigma_1-\sigma_3)$ = principal stress difference
$(\sigma_1-\sigma_3)_{ult}$ = asymptotic value of the stress difference at large axial strain
ε = axial strain
E_i = initial tangent modulus

Subbase course

The subbase material consisted of a blended mixture of crushed aggregate (67% by weight) and No. 10 crushed limestone (33% by weight). The aggregate material was obtained from a quarry near Crystal Springs about 40 miles southeast of Vicksburg. The aggregate material larger than 1-in. nominal diameter was crushed. The crushed limestone was obtained from a local supplier and originated from Kentucky. Figure 12 shows the grain-size distributions of the blending materials, the predicted distribution of the blend (red dashed line), and the measured distribution of the final blend that was used for construction (blue dashed line).

Three triaxial compression tests were conducted with the blended material under drained conditions and at confining pressures of 5, 15, and 30 psi, respectively. The tests were conducted at a controlled deformation (strain) rate. The strain rate was 1% strain per minute; the tests ended at a total deformation of 0.85 in. Figure 13 shows the Mohr's circles obtained from the triaxial test results at the different confining pressures. These data indicated an angle of internal friction of 48 deg and cohesion of 8 psi.

Figure 12. Subbase aggregate blend grain-size distributions.

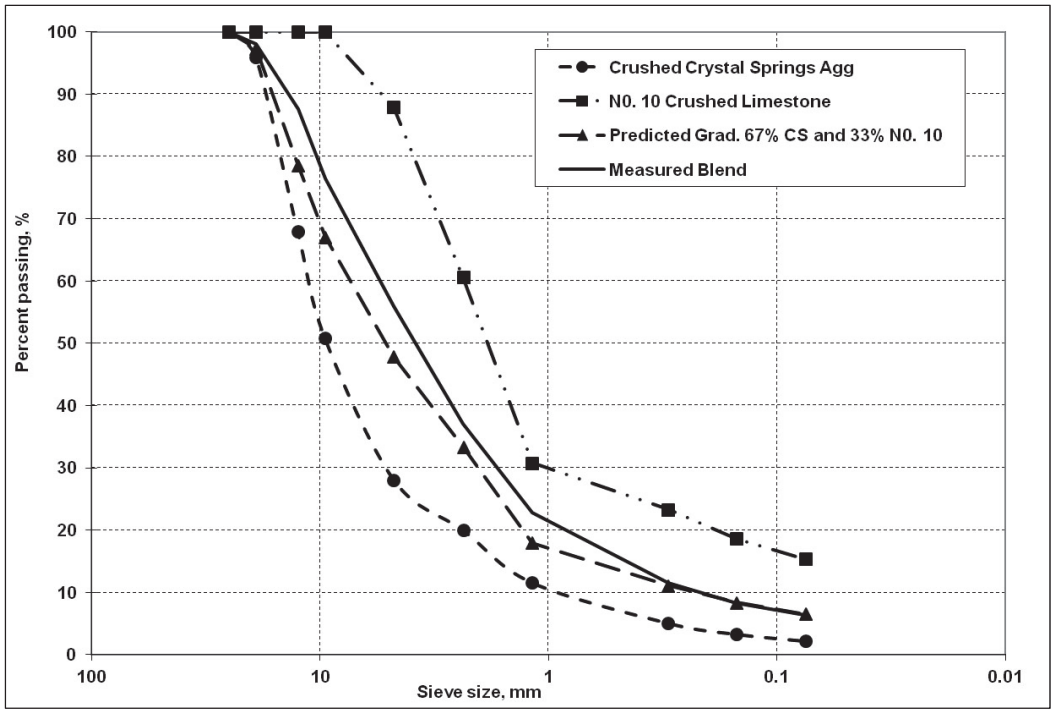

Figure 13. Mohr's circles of the subbase blend material.

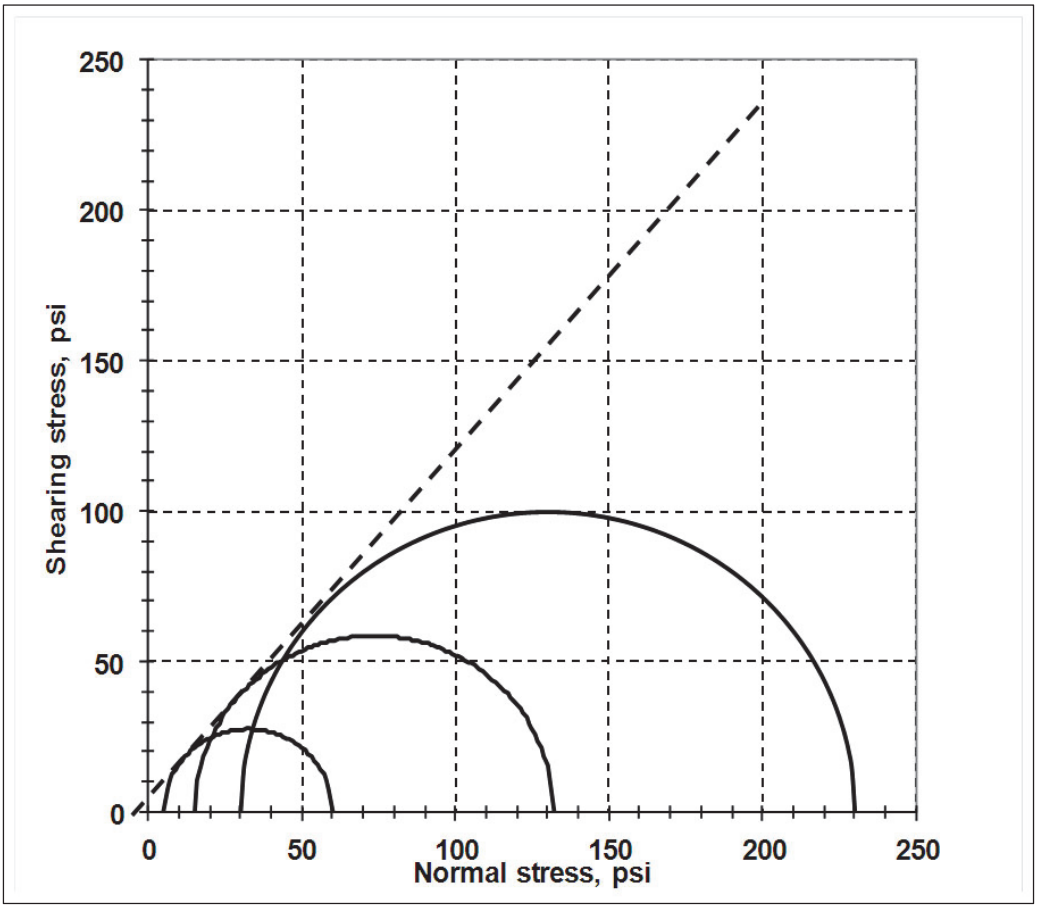

Base course

The base course for all test items was a 6-in.-thick layer of crushed limestone. Figure 14 shows the material's grain-size distribution. The material was classified as well-graded gravel (GW). Figure 15 shows the Mohr's circles obtained from the triaxial compression test results conducted at confining pressures of 5, 15, and 30 psi, respectively. The angle of internal friction was determined to be 50 deg, and the cohesion was 7 psi.

Asphalt concrete surface course

The asphalt concrete layer was 3 in. thick for each test item. The asphalt mixture was supplied by a local asphalt plant located in Vicksburg. The asphalt mixture and the layer construction were in compliance with the Unified Facility Guide Specification (UFGS) 32-12-15 standards for construction of airfield pavements, and the asphalt mixture was designed using the Marshall Design Criteria. Table 2 contains the 75-blow mix specification and the mixture characteristics used in the test sections. Table 3 contains the mixture's grain-size distribution. Figure 16 compares the mixture's grain-size distribution with the gradation limits required by the UFGS. The mixture gradation was within the UFGS gradation 2 limits except for the material passing the 9.5-mm sieve that exceeded the upper specification limit of 4.8%. Nevertheless, such excess in percentage passing was within the acceptable tolerance as indicated in the UFGS 32-12-15, Table 10. The aggregate material was classified as GW and had a specific gravity of 2.41. The nominal maximum aggregate size (NMAS) of the mixture was 9.5 mm. The asphalt content was 5.05%.

Figure 14. Base course material grain-size distribution.

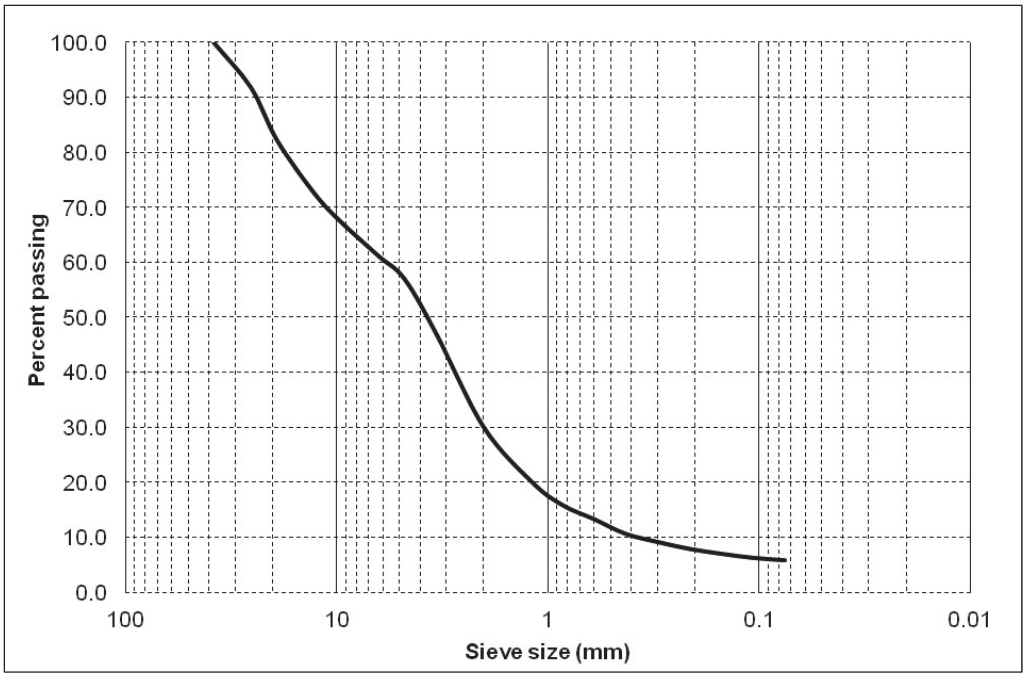

Figure 15. Base course material Mohr's circles.

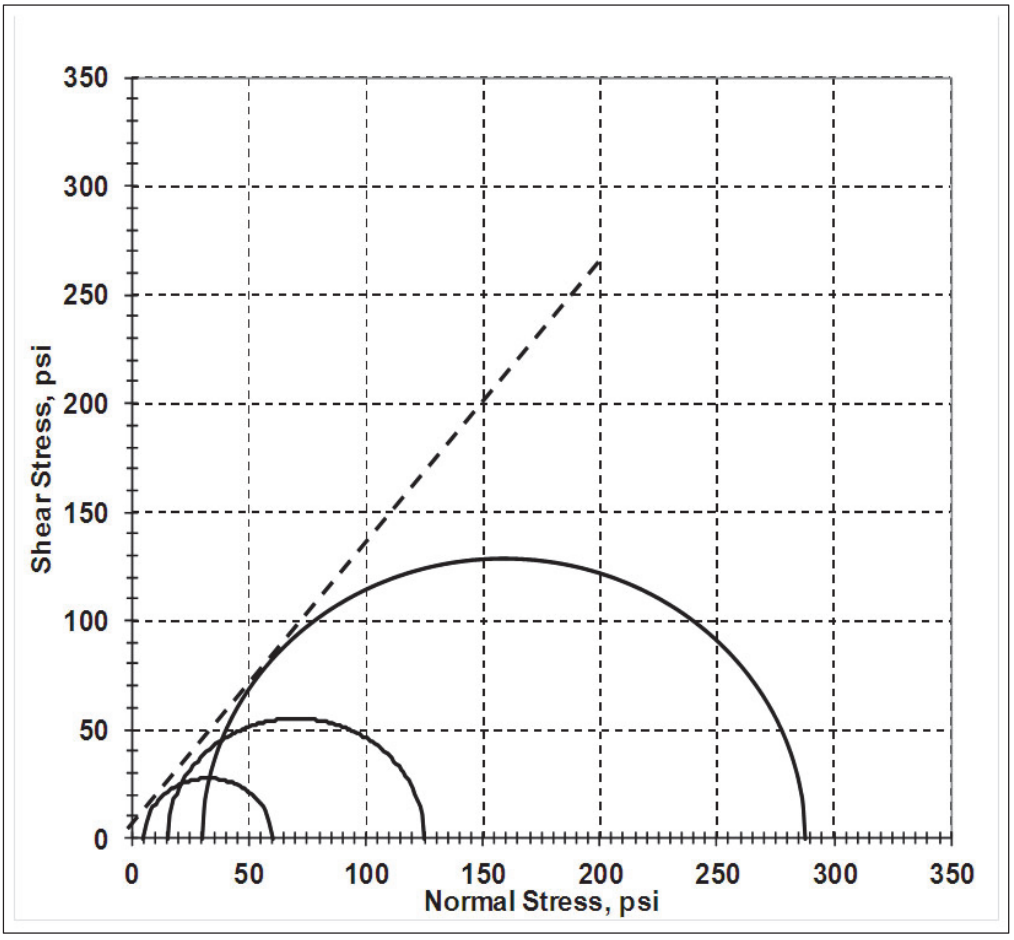

Table 2. Asphalt mixture characteristics.

Test Property	75-Blow Mix Specification	Test Section Asphalt Mixture
Min. Stability, lb	2150	2108
Flow, 0.01 in.	8 - 16	11
Air Voids, %	3 - 5	2.75
Percent Voids in Mineral Aggregate (VMA), %	13 - 15	14.1
Dust Proportion	0.8 - 1.2	1.12
Asphalt Content, %	---	5.05
Density, lb/ft^3	---	146.3
Specific Gravity	---	2.41

Table 3. Asphalt mixture grain-size distribution.

Grain Size		Asphalt Concrete
Sieve Size	Metric, mm	% Finer
1	25.4	100.0
0.75	19.0	100.0
0.5	12.5	97.2
0.375	9.5	93.8
4	4.75	65.6
8	2.36	46.9
16	1.18	36.2
30	0.6	29.5
50	0.3	16.1
100	0.15	9.7
200	0.075	5.3

Figure 16. Grain-size distribution of the asphalt mixture compared with UFGS specifications.

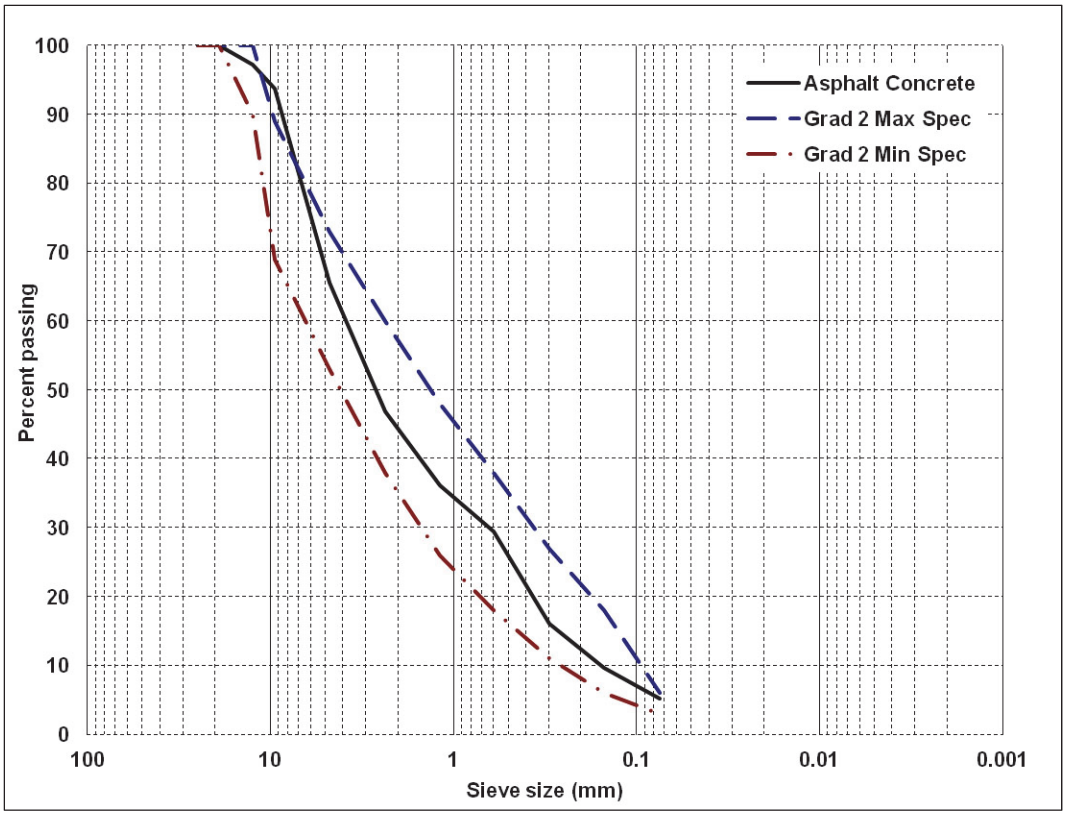

3 Construction

The test section was constructed between October 2007 and May 2008. All of the construction work was performed by ERDC personnel except for the placement of the hot-mix asphalt concrete surface. The asphalt placement was performed by a local contractor.

Excavation

The excavated area was 40 ft wide and 200 ft long with ramps on each end to facilitate equipment entry. Because the area was constructed over an under-consolidated natural silt (CL, loess), French drains were present along the entire length of the hangar at a depth of about 10 ft, with access wells for pumping water from the drains. The normal depth of the water table is less than 9 ft. Over the past half century, numerous test sections have been constructed in hangar 4, requiring excavation up to 6 ft deep. For this test section, the depth of the area to be excavated contained remnants of past test sections, which required excavation of about 5.5 ft to ensure the removal of all the non-uniform materials. The excavated area was then backfilled with 2 ft of CL to provide a stable, uniform foundation for the placement of the CH upper subgrade. A plastic moisture barrier was placed between the CL material and the processed CH subgrade material.

The CH material was placed and compacted in four lifts for the subgrade of Item 1. After placement of the CH material for Item 1, the CL fill was graded to the proper depth to allow placement of the CH subgrade for Item 2. The CH material was again placed and compacted in four lifts over a plastic moisture barrier. For Items 3 and 4, the CL layer was graded to the proper elevation to allow the placement of the CH material layer. A lift of CH material was first placed in Item 4, followed by subsequent lifts for both Items 3 and 4, which were placed at the same time to obtain a total layer thickness of 2 ft of CH material. Figure 17 shows a schematic final profile of the CL and CH layers that were constructed for this test section. Figure 18 shows the test section excavation.

Subgrade

After excavation and placement of the fill, the subgrade consisted of three distinct layers. The lower layer, at a depth greater than 5-1/2 ft, was the

native material of wind-deposited silt. Attempts to compact this layer resulted in pumping water from the high-perched water table. The material was very weak at depths greater than 2 ft below the excavated level. The CBR of the material at depths below 10 ft was estimated to be less than 2.

Figure 17. Test section subgrade final profiles.

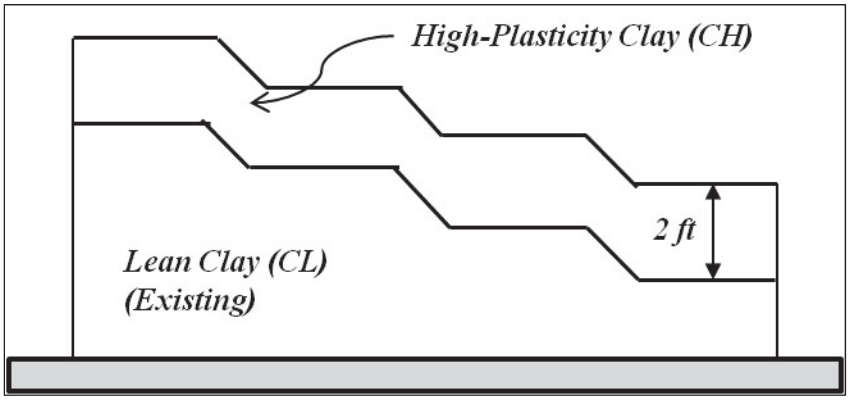

Figure 18. Test section excavation.

The layer just above the natural loess silt was the compacted CL soil that served as a construction platform and provided a uniform foundation. The thickness of the CL layer was varied to accommodate the different profiles

of the test items. The CL material was placed and compacted over the natural subgrade. In each item, the thickness of the layer was graded such that the subbase surface was at the same elevation for all items. The final subgrade layer consisted of 2 ft of a heavy clay (Vicksburg Buckshot Clay) compacted at moisture contents of 27%, 30%, and 34% to achieve the design CBR values of 15% (Item 1), 10% (Item 2), and 4% (Items 3 and 4), respectively.

The subgrade material was processed at a facility next to Hangar 4 before its placement. Material processing consisted of spreading the clay in a uniform strip to a depth of approximately 12 in. and tilling the soil with a rotary mixer to break all material clumps and ensure uniformity. The subgrade design CBR for each test item was achieved by adding water or drying the CH material to the appropriate moisture content predicted from Figure 9. Figures 19 and 20 show the material processing.

The processed CH subgrade material was then hauled to the test section and spread at a sufficient thickness to produce a 6-in.-thick compacted lift. The 2-ft-thick subgrade was placed in 6-in. lifts and compacted with three passes of an Ingram Compaction LLC rubber-tire roller (70, 000 lb with seven tires inflated at 100 psi) followed by two passes with a steel-wheel roller (DynaPac CA-25 Vibratory Compactor). After compaction, CBR tests were conducted in at least four locations per item, and moisture content samples were also obtained. Table 4 contains the CBR test results for each lift and test section item.

When the strength and moisture content of the material were not sufficiently close to the target values, the material was processed to adjust the moisture content by either adding water or allowing the material to air dry. After obtaining the correct strength (in terms of CBR) of the lift, the lift surface was scarified by lightly tilling prior to placing the next lift; this process was repeated for each subsequent lift. During the construction process, the material was not allowed to lose moisture. During breaks in the construction process, the surface of the compacted layer was lightly sprinkled with water and covered with plastic sheeting. Each test item was overbuilt a few inches to allow for the final grading of the subgrade surface prior to placement of the subbase material. After the subgrade final grading, the subgrade was sampled with a 10-in.-diam Shelby tube, and earth pressure cells (EPCs) were installed. Installation of EPCs and instrumentation will be discussed in Chapter 4. Figures 21 and 22 show subgrade placement activities.

Figure 19. Adding water to the subgrade material.

Figure 20. Subgrade material processing.

Table 4. CBR tests on the subgrade layer during construction.

	1st Lift	2nd Lift	3rd Lift	4th Lift	Surface
Item 1	14.0	12.6	13.4	13.0	15.0
	13.7	14.1	14.9	16.1	16.2
	14.9	13.0	14.3	13.2	13.8
	14.9	14.5	14.8	15.0	14.0
	15.3	14.2	13.9	13.2	13.2
	14.5	14.3	13.6	14.5	13.8
	13.0	13.0	13.8	14.5	15.5
	13.4	14.6	13.6	14.1	13.9
	13.0	14.9	13.6	13.2	15.4
	14.9	15.1	14.3	14.9	13.6
	12.6	15.3	13.8	15.2	15.9
	15.5	15.3		14.8	14.1
				Average subgrade CBR	14.2
Item 2	10.4	9.9	10.1		9.8
	9.6	9.4	10.1		10.6
	9.5	9.3	9.1		10.4
	10.0	10.3	10.4		9.5
	9.9	10.4	9.5		9.8
	9.5	10.2	10.1		10.2
	9.3	10.2	10.1		9.3
	9.6	9.9	9.4		9.5
	9.6	10.2	9.3		9.6
	9.1	9.6	10.2		9.5
	9.6	9.8	10.3		9.5
	9.7	9.5	9.1		9.2
				Average subgrade CBR	9.8
Items 3 and 4	4.2	4.4	4.0	3.8	3.8
	3.8	4.0	3.8	4.6	3.5
	3.9	4.5	3.7	3.9	3.6
	3.5	3.8	4.0	3.7	4.0
	3.7	4.5	3.7	3.5	3.8
	3.8	4.0	3.5	4.1	3.7
	3.5	4.4	3.5	4.0	3.2
	3.9	4.4	3.6	3.7	3.4
	3.8	3.9	4.4	3.6	3.3
	4.5	4.4	4.1	4.3	3.7
	3.8	3.9	4.4	4.0	3.8
	3.5	4.4	4.1	4.3	3.8
			3.4		3.1
			3.5		3.4
			3.5		3.5
					4.5
					3.8

	1st Lift	2nd Lift	3rd Lift	4th Lift	Surface
					3.7
					3.7
					3.8
					3.7
					4.2
					4.2
					4.3
					4.0
					4.2
					4.2
					3.9
					4.8
					3.3
					3.6
					4.3
					4.1
				Average subgrade CBR	3.9

Figure 21. Subgrade material placement.

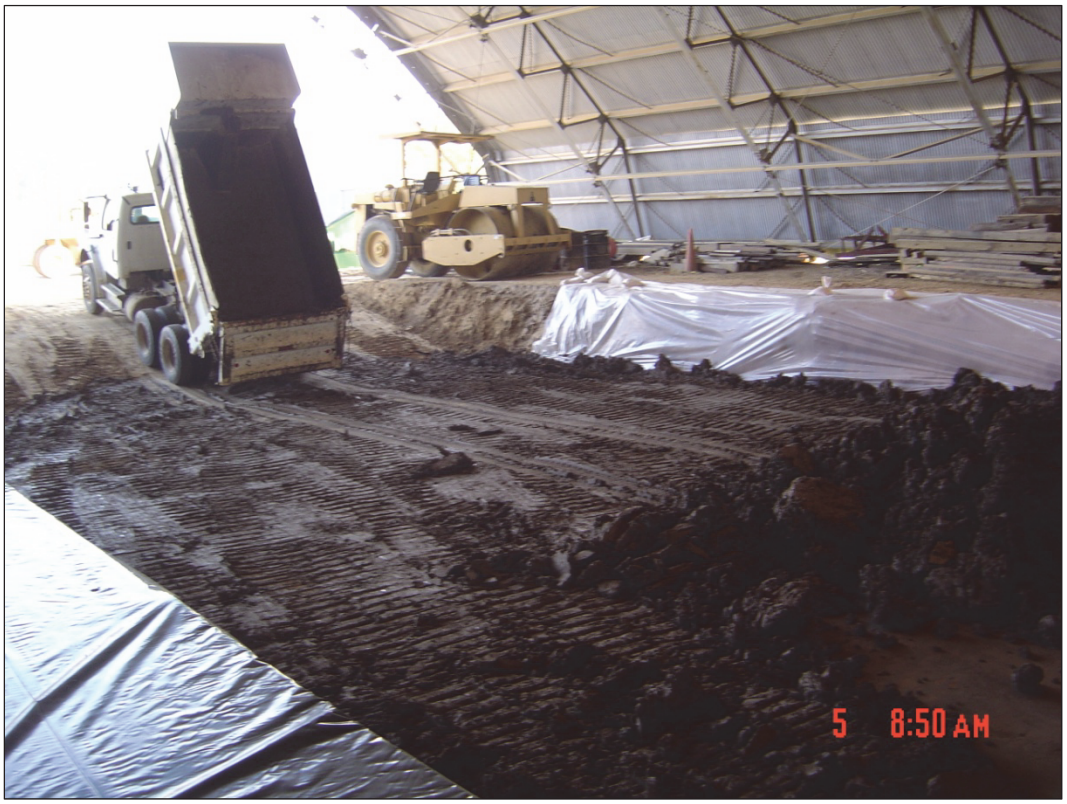

Figure 22. Subgrade layer covered after compaction.

Subbase course

The subbase material, a blended mix of 67% crushed aggregate (Figure 23, left) and 33% No. 10 crushed limestone (Figure 23, right), was placed in lifts to total thicknesses of 7 to 23 in. to achieve the required design thicknesses. The subbase material was delivered by dump trucks and placed in 5- to 7-in.-thick lifts. Each lift was compacted by 22 passes of a vibratory steel-wheel roller. Target moisture content to achieve 100% modified Proctor compaction was 3.5%. During compaction, the subbase material was kept moist by sprinkling each lift with water prior to each pass of the vibratory roller. Figures 24 and 25 show stockpiled subbase material and subbase construction activities, respectively.

The dry density, wet density, and moisture content of the subbase material were monitored during compaction to determine at what pass level the material would achieve maximum density. A nuclear gauge was used to obtain measurements of density and moisture in accordance to ASTM D-6938-10. Maximum density was achieved after approximately 16 to 18 passes of the self-propelled vibratory steel roller. The moisture content remained constant at about 3.5% during placement. Figure 26 shows dry

Figure 23. Material included in the subbase blended mix: crushed aggregate (left) and crushed limestone (right).

Figure 24. Blended subbase material stockpile.

Figure 25. Subbase placement activities.

Figure 26. Subbase material field characteristics.

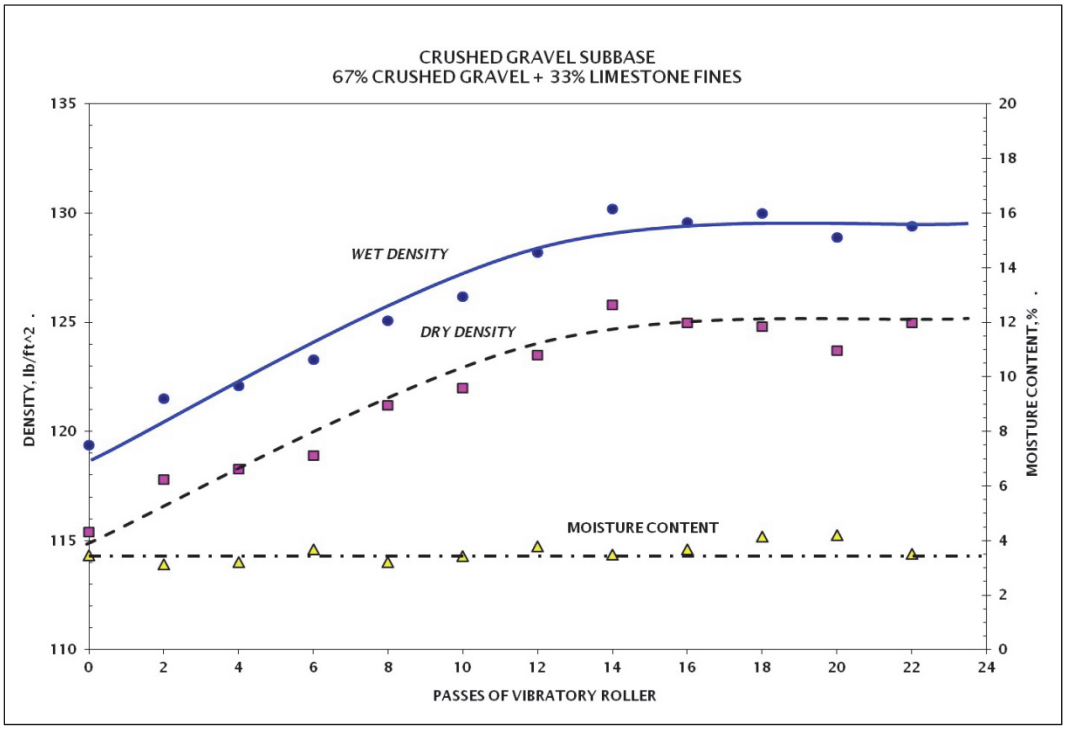

density, wet density, and moisture content values as a function of the number of passes of the vibratory roller. Table 5 contains the measured values of density (wet and dry) and moisture content in relation to the number of passes of the vibratory roller. CBR tests were executed after placement and final compaction of the granular material. Table 6 contains the CBR test results for each test item.

Table 5. Subbase soil characteristics as function of passes of the vibratory roller.

Passes	Wet Density, lb/ft²	Dry Density, lb/ft²	Moisture Content, %
0	119.40	115.40	3.47
2	121.50	117.80	3.14
4	122.10	118.30	3.21
6	123.30	118.90	3.70
8	125.10	121.20	3.22
10	126.20	122.00	3.44
12	128.20	123.50	3.81
14	130.20	125.80	3.50
16	129.60	125.00	3.68
18	130.00	124.80	4.17
20	128.90	123.70	4.20
22 (final values)	129.40	125.00	3.52

Table 6. CBR test results for the subbase layer.

Item 1	Item 2	Item 3	Item 4
26.3	20.8	15.0	18.0
24.2	20.8	15.0	18.0
24.8	20.8	16.5	19.0
26.9	21.1	7.0	82.9
28.4	21.4	7.7	84.4
27.5	22.3	7.6	86.9
18.3	17.4	9.2	65.4
21.4	17.7	8.9	63.3
20.2	18.0	10.1	61.2
16.2	22.9	24.2	23.9
15.9	23.9	21.7	21.4
15.6	23.9	19.9	25.1
			30.6

Item 1	Item 2	Item 3	Item 4
			31.2
			30.3
			15.3
			15.6
			13.5
Average subgrade CBR (final values)			
22.1	20.9	13.6	39.2

Base course

The base course was a 6-in.-thick layer of ASTM 568 crushed limestone. Figure 27 shows the placement process of base course material. The base lift was compacted by 16 passes of a self-propelled vibratory steel roller. Figure 28 shows dry density, wet density, and moisture content values as a function of the number of passes of the vibratory roller following the same procedure used for the subbase material. The base material achieved maximum density in about 10 passes of the vibratory roller. Moisture content remained constant at approximately 3% during placement. Table 7 contains the measured values of density (wet and dry) and moisture content in relation to the number of passes of the vibratory roller. CBR tests were executed after placement and final compaction of the granular material. Table 8 contains the CBR test results for each test item.

Asphalt concrete

The asphalt mixture was provided and placed by a local asphalt contractor. Paving operations started on 14 Jan 2008. The air and ground temperatures were 60°F. The temperature of the asphalt mix at the plant was 300°F. When the mix reached the site, the asphalt temperature was between 285°F and 295°F. After compaction, the asphalt mat had a temperature of 270°F.

The asphalt mixture was placed in a 4-in.-thick lift and compacted to a thickness of 3.25 in. The density of the compacted layer was between 135 and 141 pcf. The asphalt layer was placed in the three paving lanes in the north-south direction. The lanes had widths of 13, 13, and 14 ft for Lanes 1 through 3, respectively, and a length of 200 ft. Figures 29, 30, and 31 show some of the paving operations. After placement, the asphalt layer was allowed to cure for one month before the application of any test traffic.

Figure 27. Base layer placement.

Figure 28. Base material field compaction characteristics.

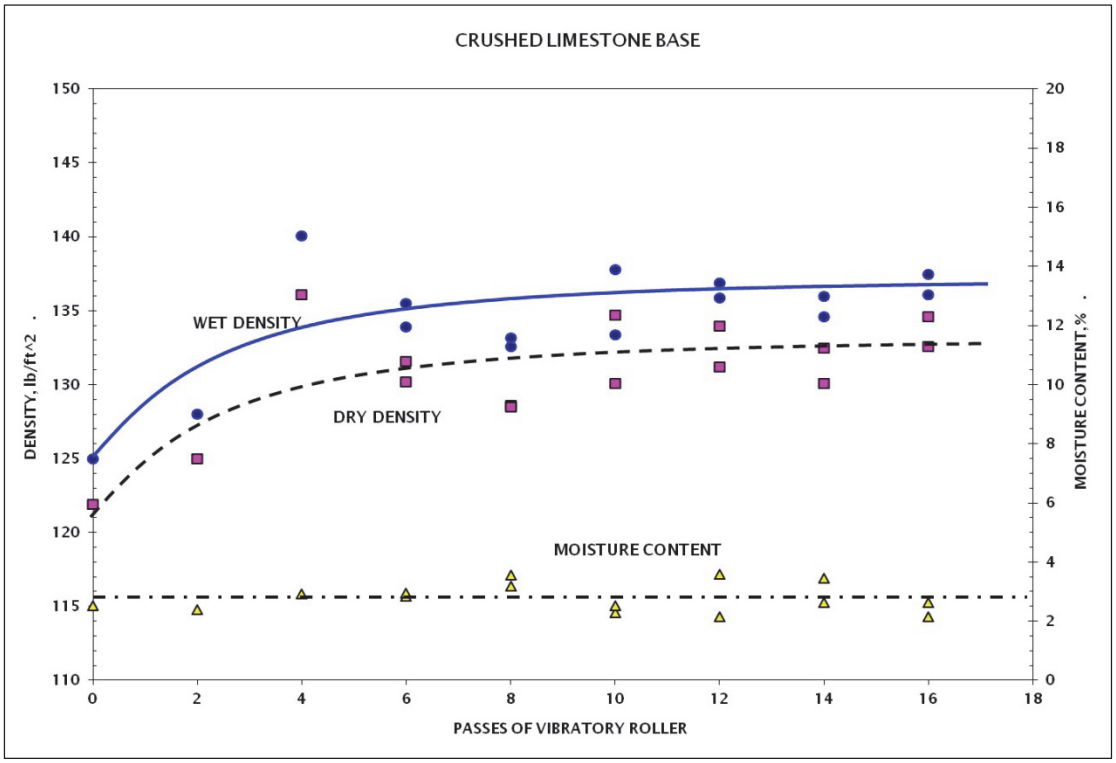

Table 7. Base soil characteristics as function of passes of the vibratory roller.

Passes	Wet Density, lb/ft²	Dry Density, lb/ft²	Moisture Content, %
0	125.00	121.90	2.54
2	128.00	125.00	2.40
4	140.10	136.10	2.94
6	133.90	130.20	2.84
6	135.50	131.60	2.96
8	133.20	128.60	3.58
8	132.60	128.50	3.19
10	137.80	134.70	2.30
10	133.40	130.10	2.54
12	135.90	131.20	3.58
12	136.90	134.00	2.16
14	134.60	130.10	3.46
14	136.00	132.50	2.64
16	136.10	132.60	2.64
16 (final values)	137.50	134.60	2.15

Table 8. CBR test results for the base layer.

Item 1	Item 2	Item 3	Item 4
41.3	24.5	21.1	41.0
35.5	31.2	22.0	44.3
39.8	27.5	18.3	38.8
48.3	32.1		
Average subgrade CBR (final values)			
41.2	28.8	20.5	41.4

Figure 29. Paving operations, mat placement.

Figure 30. Paving operations, break-down rolling.

Figure 31. Paving operations, rubber-tire roller compaction.

Testing and sampling

CBR testing was conducted at several locations on each granular layer and in each test item. Table 9 summarizes the average CBR values that can be considered pre-traffic. This testing was accomplished prior to the placement of the asphalt layer. The complete set of test data is provided in Appendix A.

Table 9. Pre-traffic average CBR values.

Pavement Layer	Item 1	Item 2	Item 3	Item 4	Average for Traffic Lane
Base	41.2	28.8	20.5	41.4	33.0
Subbase	22.1	20.9	13.6	39.2	24.0
Subgrade	14.2 (15)	9.8 (10)	3.9 (4)	3.9 (4)	

Note: Values in parentheses represent target CBR values.

Each layer was tested with a Falling Weight Deflectometer (FWD). These deflection test results are included in Appendix A.

Elevation measurements also were obtained after completion of each pavement layer. Figure 32 shows the plan view of the profile points for the subgrade, subbase, base, and surface layers, respectively. Figure 33 shows a plot of all the elevation data for each section item and the position within the layer of the EPC and single-depth deflectometer (SDD) sensors. The horizontal lines within each item represent the average interface location between pavement layers. Table 10 summarizes layer thickness (target and as-built) and average deviation (in absolute value) from the reference elevation. EPCs and SDDs were installed about 3 in. below the base, subbase, and subgrade interfaces to avoid breakage of the sensors during construction and compaction procedures.

Figure 32. Plan view surface profile points for each layer.

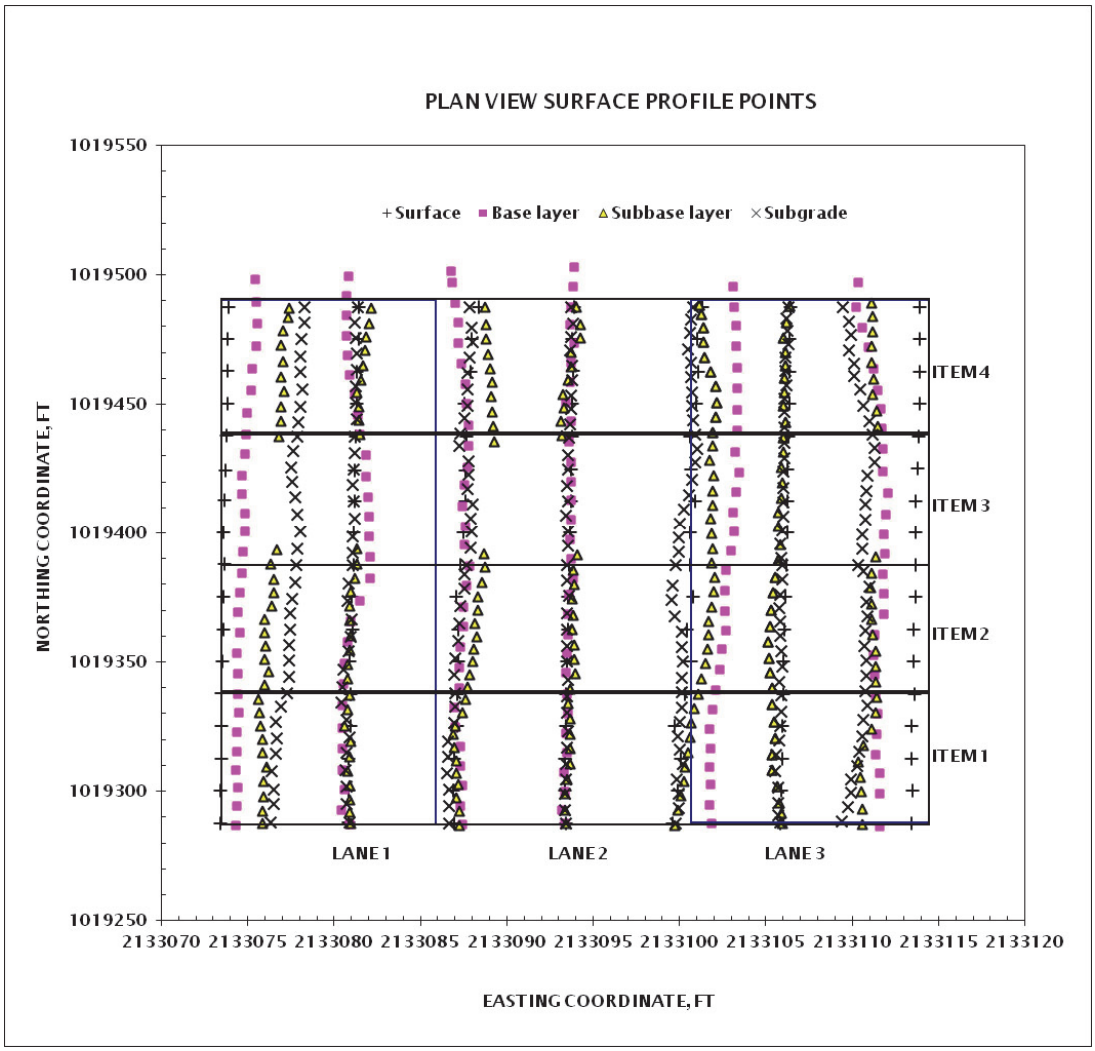

Figure 33. Elevation data for each layer and sensor location.

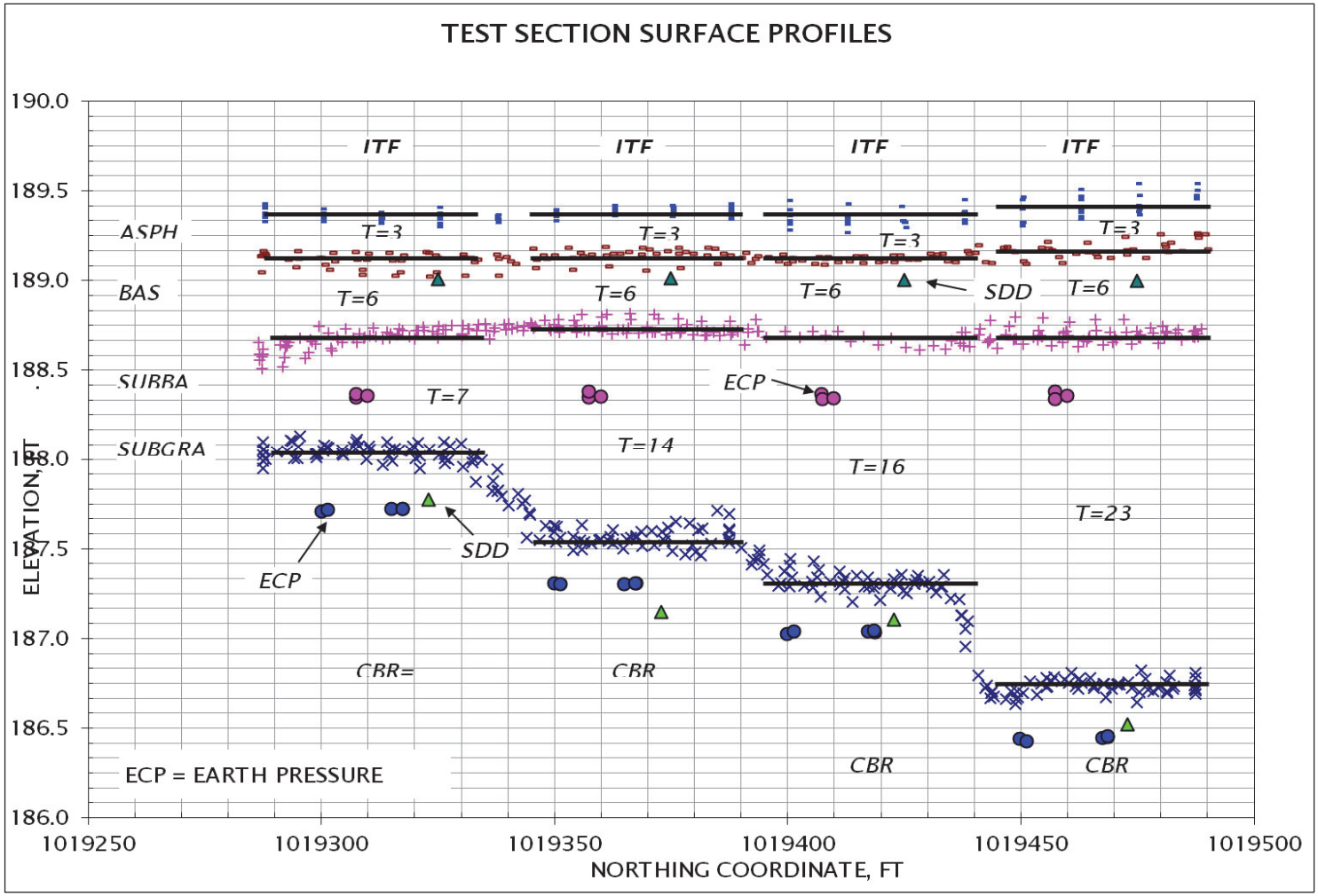

Table 10. Reference elevation average deviation (absolute value).

Pavement Layer	Subgrade	Subbase Layer	Base Layer	Surface
Target thickness, (in.)	n/a	6 (Item 1) 14 (item2) 16 (Item 3) 23 (Item4)	6	3
As-built thickness	n/a	7 (Item 1) 14 (item2) 16 (Item 3) 23 (Item4)	6	3
Deviation in elevation (in.)	0.44955	0.44984	0.4433	0.4824

4 Instrumentation

Instrumentation was installed throughout the test section to monitor pavement performance under traffic. The instrumentation included temperature sensors, EPCs, SDDs, and surface strain gauges.

Temperature sensors

Eight temperature sensors were installed in the test section at four locations. The sensors (I-button), manufactured by The Transtec Group, Inc., Austin, Texas, are self-contained, programmable units capable of reading temperature for up to two years, depending on the data collection frequency. At each location, one sensor was mounted at a depth of about 3 in., corresponding to the bottom of the asphalt layer, while another sensor was installed just below the asphalt surface. A mixture of asphalt and sand was used to initially place and protect the sensors within the asphalt layer. Two sensors, used to measure air temperature, were installed approximately 5 ft above the pavement surface and located specifically on the north and south ends of the test section. Figure 34 shows sensor locations within the test section.

Earth pressure cells

The EPCs were manufactured by Geokon, Lebanon, New Hampshire. The model 3500 was circular with a diameter of 9 in. The EPC consisted of two stainless steel plates welded together around the edge and leaving a narrow space within, which was filled with de-aired hydraulic oil. The space was hydraulically connected to a pressure transducer that converted the oil pressure to an electrical signal transmitted through a signal cable to the data logger. The pressure transducers had a voltage output range of 0-5 V DC and were attached to the data cable with a sealed, water-resistant connection.

Two EPCs were installed in each test item. In Item 1 of Lanes 1, 2, and 3, 200-psi-capacity cells were placed about 3 in. into the subbase and 100-psi-capacity cells were placed about 3 in. into the subgrade. In Items 2, 3, and 4 of Lanes 1, 2, and 3, 200-psi-capacity cells were placed about 3 in. into the subbase, and 60-psi-capacity cells were placed about 3 in. into the subgrade.

Figure 34. Temperature sensor locations.

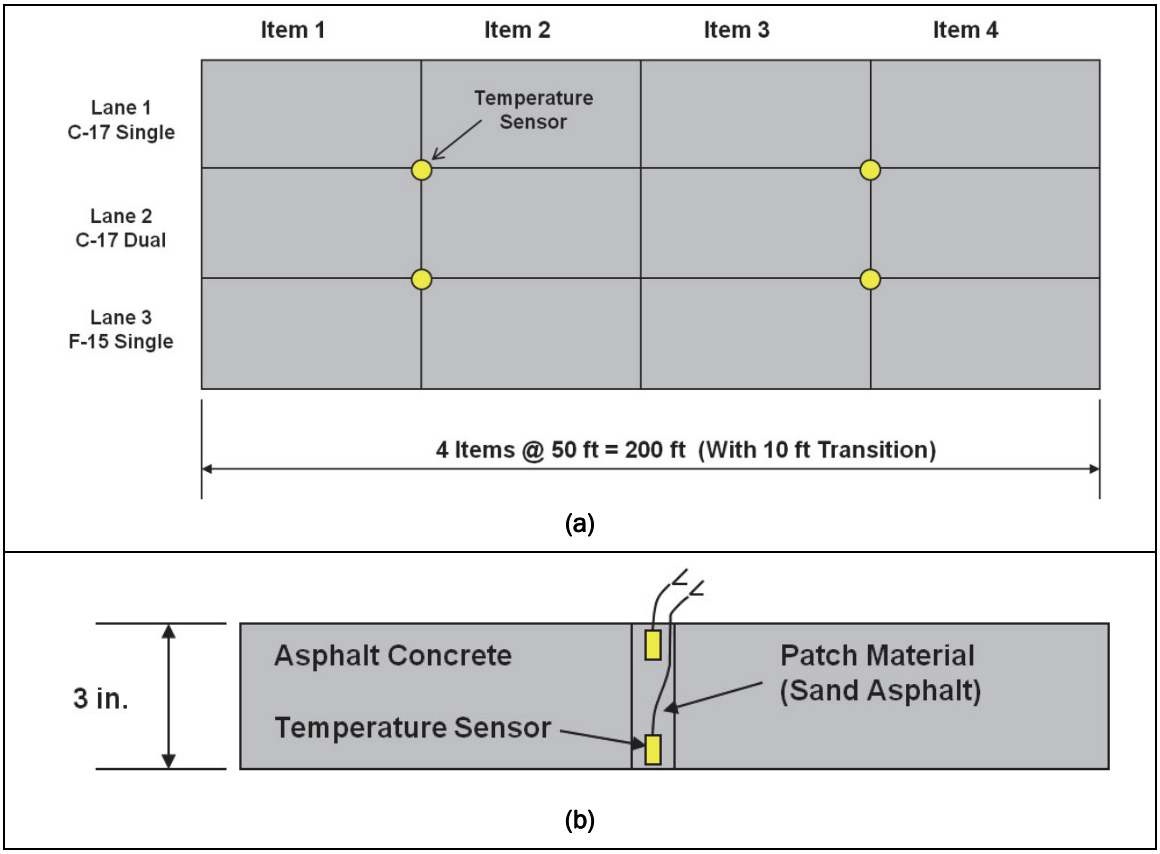

In addition, all the items of Lane 2 were also instrumented with two additional EPCs to measure horizontal pressure. These EPCs were located on the center lane on the subgrade. Figure 35 shows the EPC locations for each lane and item. To assure continuous contact between the cell plates and the soil, the cells were backfilled with a thin layer of sand material.

Single-depth deflectometer

Single-depth deflectometers (SDDs) were custom built for this full-scale testing. The sensor measured displacement and consisted of a linear variable differential transformer (LVDT) mounted on a spring; the sensor had a range of ±1 in. Figure 36 shows an SDD after installation. Two SDDs were installed in each item of Lane 2 and located 3 in. below the asphalt layer and at the top of the subgrade, anchored at a depth of 10 ft below the pavement surface.

Figure 35. Instrumentation locations. Note: blue shapes = ECP; green shapes = SDD (continued).

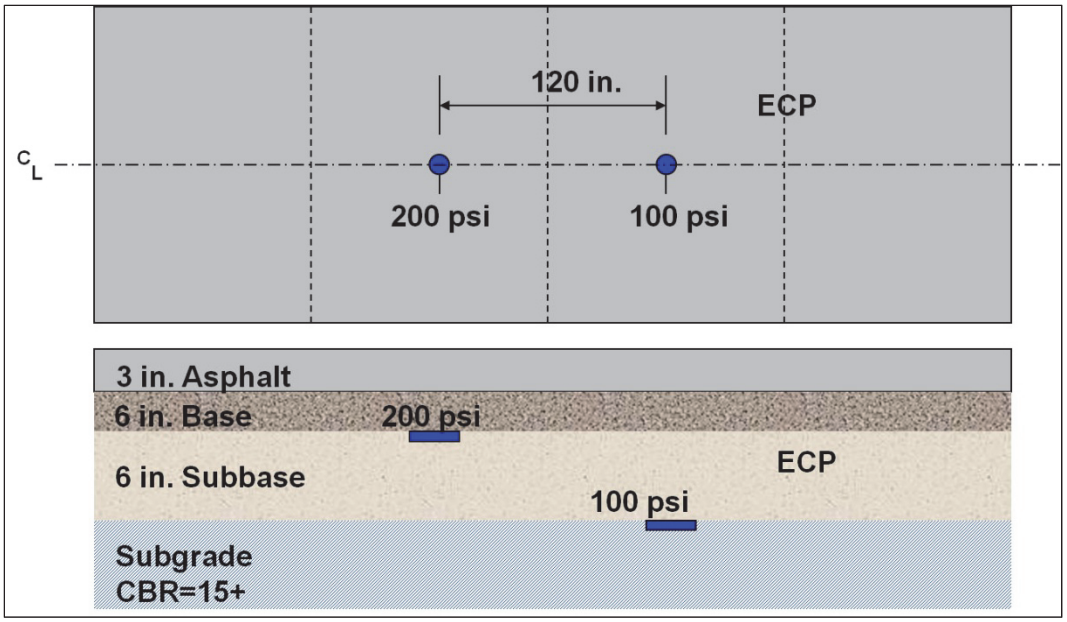

(a)

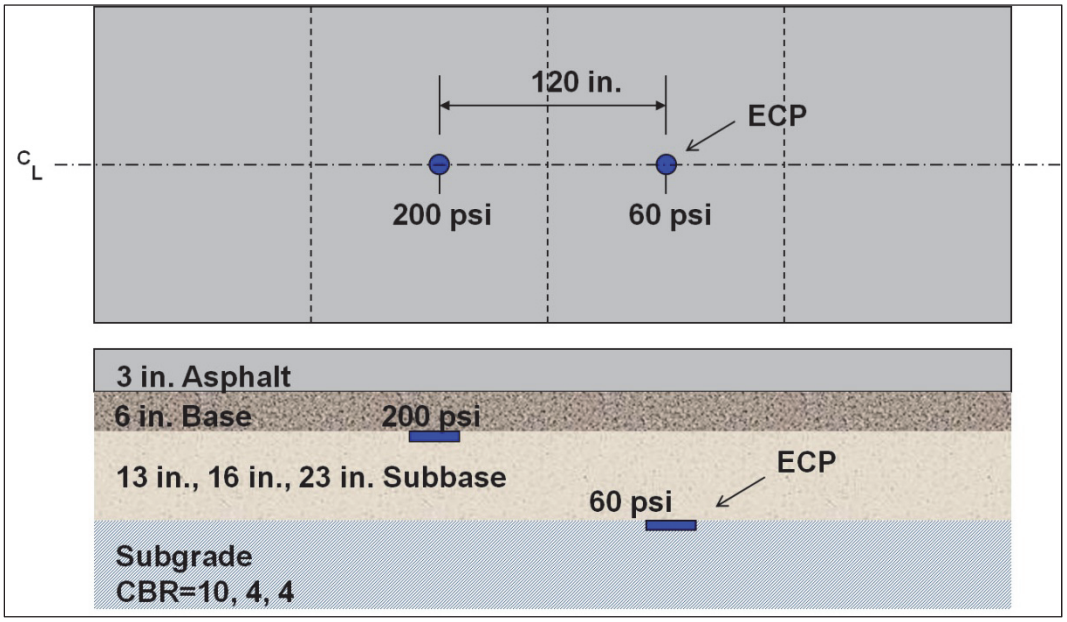

(b)

Figure 35. (concluded).

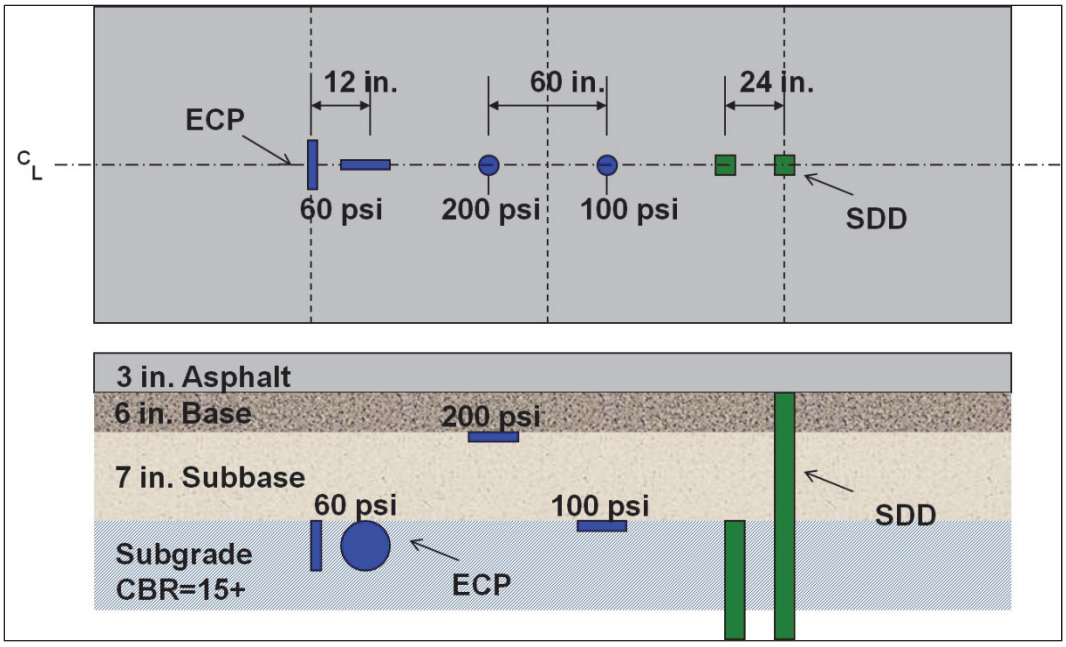

(c)

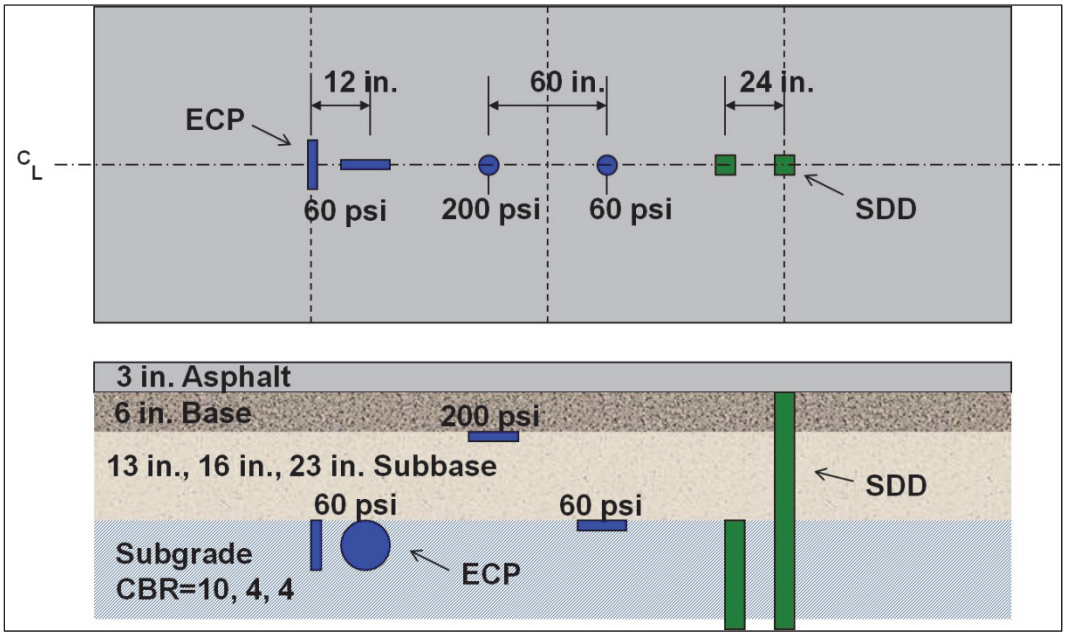

(d)

Figure 36. SDD after installation.

Strain gauges

Eight surface strain gauges were positioned on Lane 1, Item 4: four were parallel to traffic and four were transverse to traffic. Figure 37 shows the position of the gauges on the pavement surface. The 2-in.-long gauges were manufactured by Vishay, Precision Group, Wendell, North Carolina. The strain gauges were serviceable only during the rolling tests prior to trafficking the lane item. The impact of the high pressure tire moving over the gauges limited gauge functionality.

The general procedure for installation of the gauges was the following:

1. The asphalt surface was first cleaned and lightly sanded.
2. A thin film of a quick-setting epoxy was applied to the surface and allowed to completely cure.
3. The epoxy surface was then sanded such that only a very thin film of epoxy remained on the asphalt surface.
4. The foil strain gauges were bonded to the epoxy surface.
5. Thin wire leads were attached to the gauges.

6. The gauges and connections were covered with a rubber-cement coating to provide water protection.
7. A shielded instrumentation cable was attached to the strain gauge leads.
8. To provide additional protection from traffic, the gauges and connections were covered with a thin rubber pad that was taped to the asphalt surface.

Figure 37. Strain gauge locations on Lane 1 Item 4.

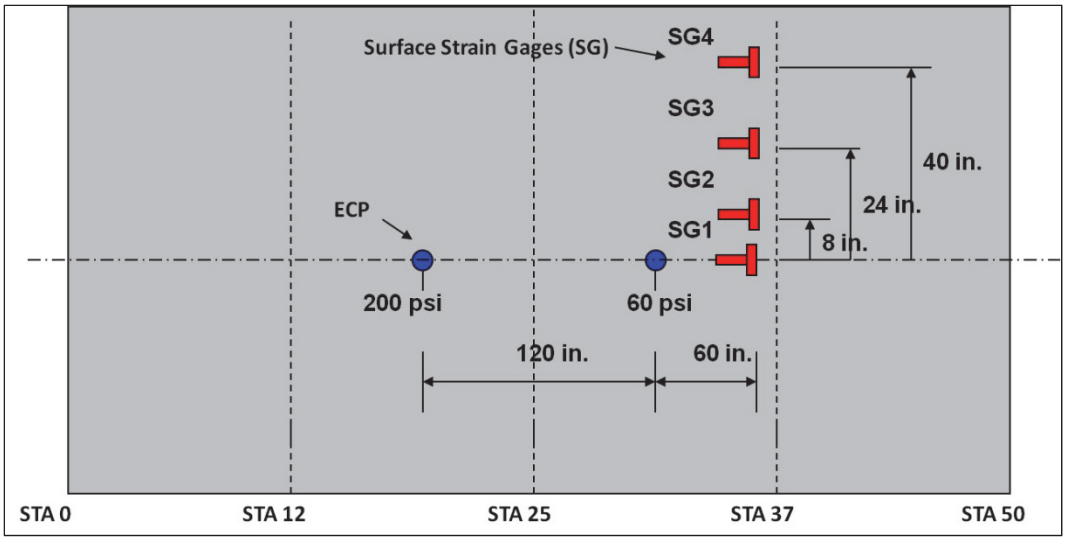

5 Testing Characteristics

The test section was trafficked on three separate lanes, 40 ft wide by 200 ft long. Traffic included medium and heavy loads, high (F-15E) and low (C-17) tire pressures. Gear configurations included both single and dual. Each test item was trafficked individually with the heavy vehicle simulator – aircraft (HVS-A) Mark V, manufactured by Dynatest International, and the number of passes to failure was recorded.

The heavy vehicle simulator

The HVS-A (Figure 38) was employed to simulate each aircraft load. The actual HVS-A travel length while trafficking is 40 ft. The HVS-A has the capability of applying loads up to 100,000 lb with single-wheel or dual-wheel gear configurations. The test gear is mounted in a carriage that moves along a horizontal beam attached to the HVS-A frame. The gross weight of the HVS-A acts as a reaction force when applying the load to the test gear. The carriage is hinged at one end with a hydraulic ram applying the load at the other end. The movement of the carriage, both laterally and longitudinally, and the hydraulic ram pressure are pre-programmed and controlled by a computer. The carriage has the capability of moving 40 ft in the longitudinal direction and 48 in. in the transverse direction. With a 48-in. limitation on the transverse movement of the carriage, the maximum traffic lane width would be 48 in. plus the distance from the centerline of the gear to the outside tire. The transverse movement of the carriage can be programmed to move laterally either by lifting the gear at the end of the test section and repositioning the gear at the next lateral interval position or by moving it laterally along the lane during trafficking. The gear lifting is more time consuming but results in wheel paths that are parallel with the HVS-A frame and traffic lane. During the traffic tests, both methods of moving the carriage transversely were utilized. Traffic was applied in a distributed pattern over a lateral wander width of 4 ft plus the width of the test gear and in bidirectional fashion in the longitudinal direction. The HVS-A traveled at an approximate speed of 5 mph.

Test lanes and traffic patterns

While a test item is a portion of the entire test section, the traffic lane is an area of the pavement surface of a given width extending through the length of the test section. Thus, a traffic lane would extend across all four test

Figure 38. Heavy Vehicle Simulator (HVS-A) used for traffic testing.

items. The test section was divided into three traffic lanes to apply traffic with the F-15E single tire, the C-17 single tire, and the C-17 dual-tire gear. The nominal widths were 5 ft, 10 ft, and 5 ft for traffic lanes 1, 2, and 3, respectively, with 5 ft of buffer strip between each lane and a 5-ft clearance at each end of the test section. Figures 5 and 39 show the section layout with an indication of the traffic lanes. Figure 40 shows the single- and dual-tire assemblies used for the testing.

Lane 3 was trafficked with the F-15 tire. The tire was loaded to 35,235 lb with an internal tire pressure of 325 psi. This loading and tire pressure yielded a computed contact area of 108 in^2. The measured contact area had a width of 8.8 in. and a length of 15 in. The computed area, based on the assumption of an elliptical shape, was 104 in^2. The contact area for this tire was slightly squarer than an ellipse; thus, the computed elliptical area would be slightly lower than the actual contact area (Figure 41). Nevertheless, it was concluded that the approach of using the tire load and tire pressure to compute an elliptic contact area was sufficiently accurate for design and evaluation.

Figure 39. Section layout with traffic lane details.

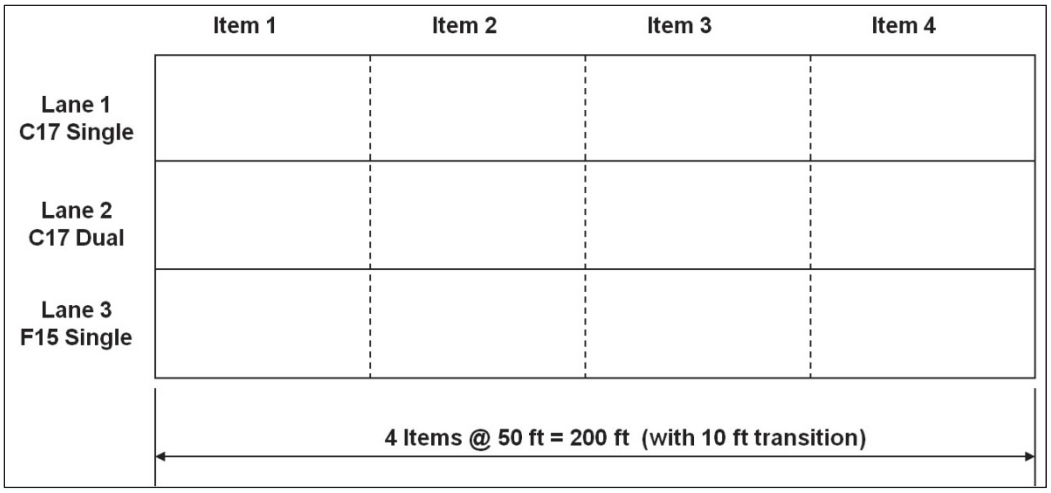

Figure 40. Single F-15E gear (left) and dual C-17 gear (right) tire assemblies.

Figure 41. F-15 tire imprint.

For each lane, the trafficking was applied in a laterally distributed pattern. A pattern is a completely repeatable set of tire or gear movements across a pavement. For Lane 3, the traffic pattern was over a lateral wander width of 4 ft and bidirectional in the longitudinal direction. The 4-ft wander width resulted in a 64.8-in. width of pavement being trafficked. The traffic pattern began with the tire located at one corner of the traffic lane. Four longitudinal passes were made along the first tire path. After completion of the four passes, the tire was moved laterally 8 in. The process was repeated until the carriage reached the opposite side of the traffic lane. The sweep across the traffic lane resulted in seven wheel paths (28 tire passes), which resulted in four coverages for 100% of the traffic lane. After reaching the opposite side of the traffic lane, the tire was lifted and moved laterally 4 in. (1/2 of a wheel path) back toward the beginning side to establish the beginning of the second sweep. The second sweep was one wheel path less than the previous sweep and included six wheel paths. This sweep resulted in an additional four coverages for the center 48.8 in. of the traffic lane. The process of moving the tire laterally 4 in. toward the center area, narrowing the trafficked area at every sweep, was repeated to obtain sweeps of five and four wheel paths. The completion of the sweep for the four wheel paths completed the traffic pattern and resulted in a total of 88 passes for 16 coverages over the center 40.8 in. of the traffic lane. Since the 88 passes resulted in 16 coverages, the pass-to-coverage ratio for the traffic pattern was 5.5. Figure 42 shows a graphical depiction of the traffic pattern used for the single-tire F-15 traffic lane.

Lane 2 was trafficked with the dual-wheel assembly of the C-17 tire. The dual tires had a center spacing of 40.5 in. Each tire was loaded to 43,360 lb at a tire pressure of 142 psi. This loading and tire pressure resulted in a computed contact area of 305 in^2. The tire print measured 17.2 in. wide and 22.0 in. long. With the assumption of an elliptical-shaped area, the computed area of the tire print was 297 in^2. This tire, like the one employed for the F-15, had a slightly square shape; thus, the assumption of an elliptical-shaped contact area produced a slight underestimation of the effective tire contact area (Figure 43).

The carriage lateral movement of the dual-tire assembly was similar to that for the F-15 single tire. Because of the dual-tire arrangement, the C-17 dual assembly resulted in a much wider trafficked area. For traffic lane 2, the carriage was moved 16 in. for each lateral shift. The 16-in. shift produced two sets of four wheel paths, resulting in a pavement width of 105.7 in.

Figure 42. Normally distributed traffic pattern for the F-15 single tire.

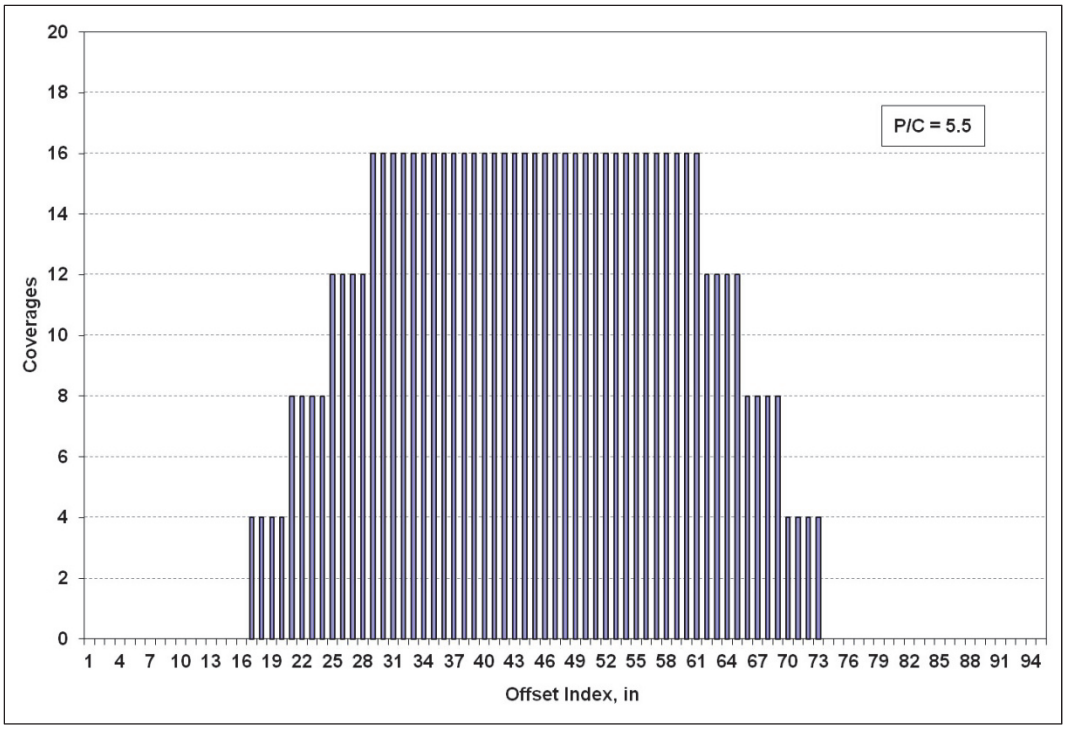

Figure 43. C-17 tire imprint.

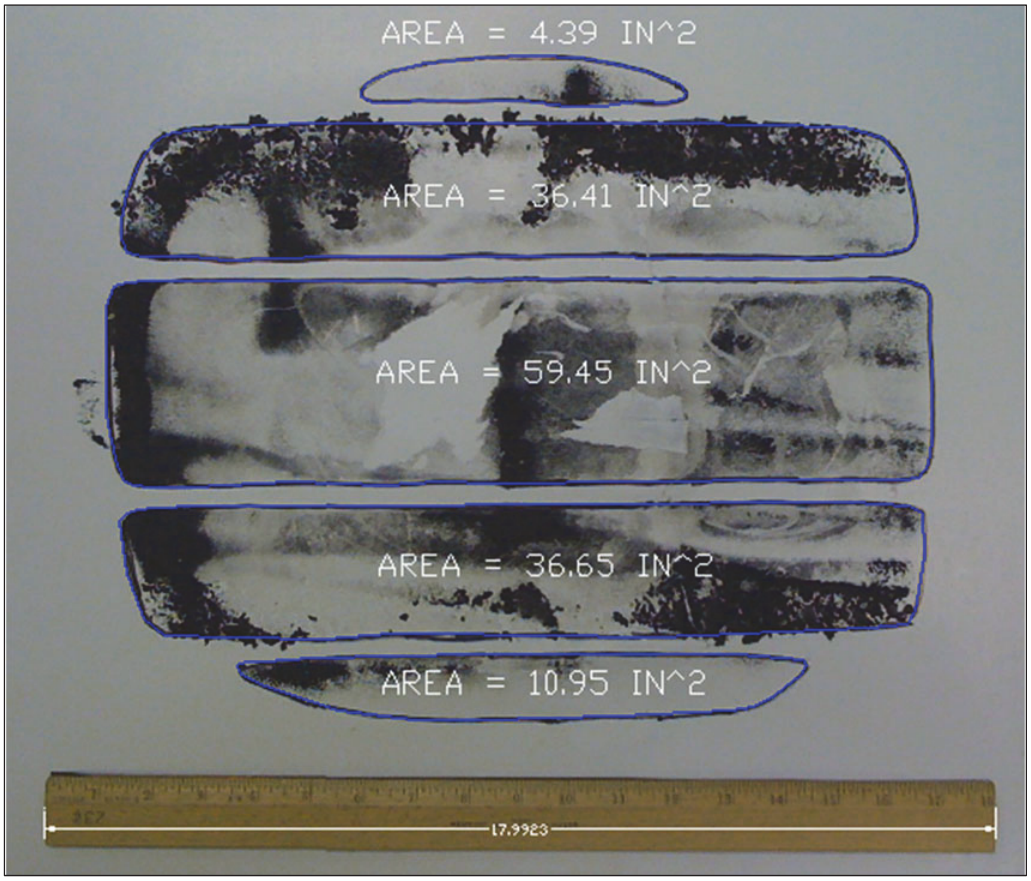

actually receiving traffic. With four wheel paths for each tire, the first sweep of the carriage resulted in 16 passes, the second sweep (three wheel paths) resulted in 12 passes, and the third and the fourth sweeps produced 8 and 4 passes, respectively, for a total 40 passes. This traffic pattern applied 16 coverages to the center 57.7 in. of the traffic lane. This resulted in a pass-to-coverage ratio equal to 2.5. Figure 44 shows the traffic pattern for the C-17 dual gear.

Figure 44. Traffic pattern for the C-17 dual-tire gear.

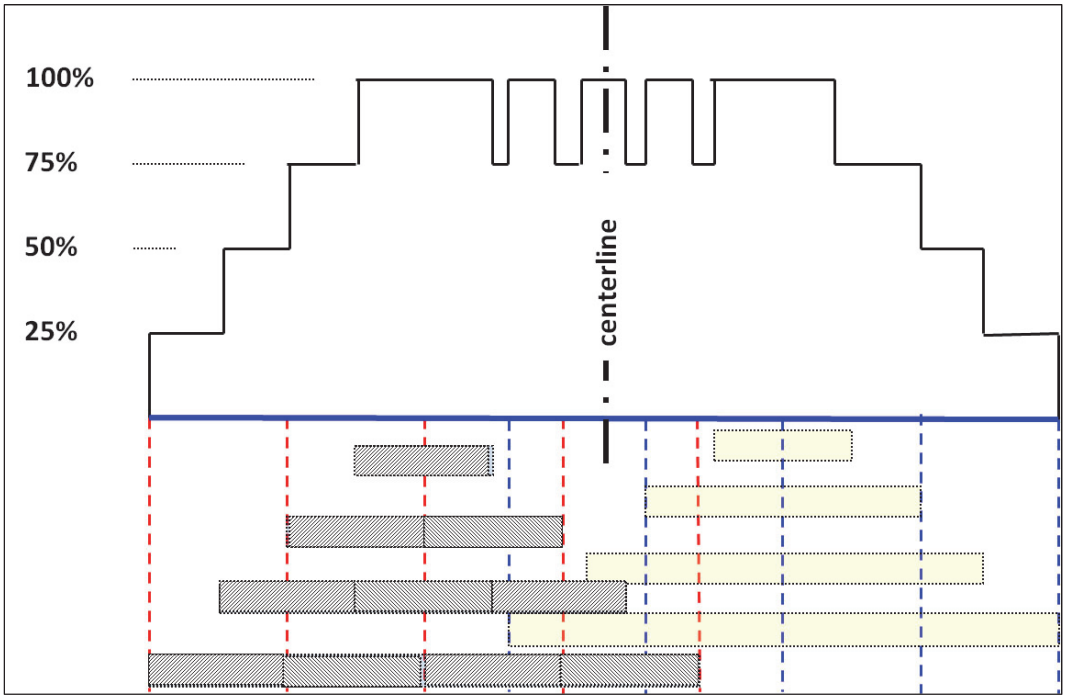

Lane 1 was trafficked with the C-17 single-wheel gear. The single C-17 tire had the same loading and tire pressure as the dual C-17 gear. The trafficked area was identical to one-half of the dual-wheel traffic area, with the exception that the trafficked area was shifted to the center of the traffic lane. The width of the trafficked area was 65.2 in. The lateral shift of the carriage was 16 in., giving four wheel paths for the first sweep, three wheel paths for the second sweep, two wheel paths for the third sweep, and one wheel path for the fourth sweep. This traffic pattern required 40 passes and resulted in 16 coverages for pass-to-coverage ratio of 2.5 (Figure 45).

Figure 45. Normally distributed traffic pattern for the C-17 single tire.

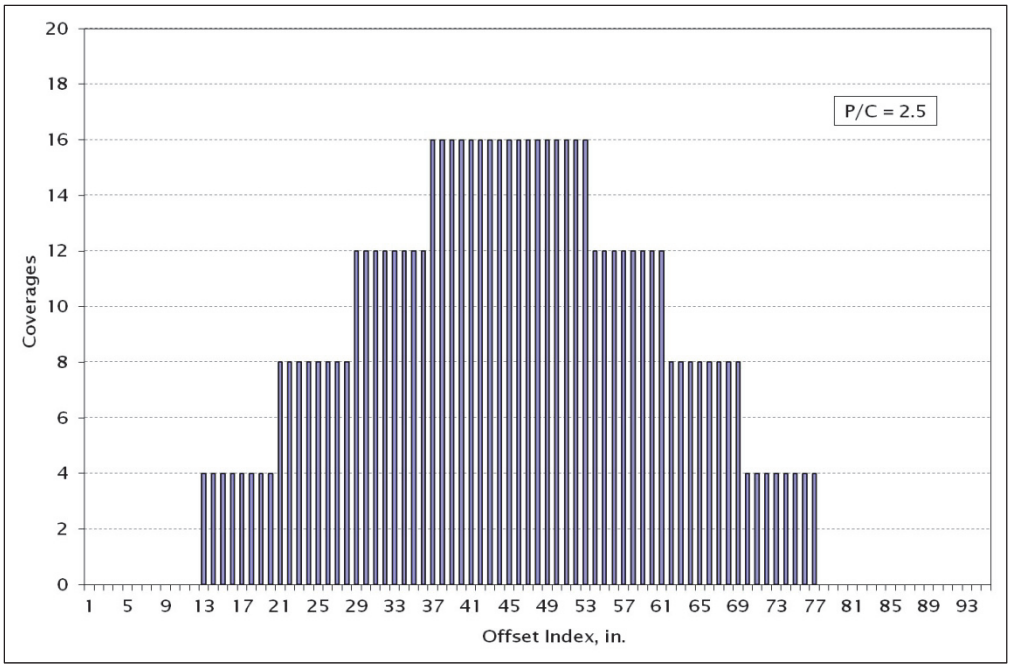

HVS-A calibration

The HVS-A was calibrated prior to traffic to ensure the correct loading was applied (Figure 46). The HVS-A applies the load through a hydraulic ram and lever arm system.

Figure 46. HVS–A calibration.

The load applied to the tire was determined by measuring the oil pressure supplied to the hydraulic ram. Since there was no independent system to directly measure the load being applied to the test tire, a calibration of the ram and mechanical advantage of the carriage level arm was considered necessary. To perform this calibration, load cells were used to verify the HVS-A loading, and strain gauges were installed on the lever arm of the HVS-A carriage and on the tire axle. Three load cells measured the load applied to a single tire, and four load cells were used with the C-17 dual tires. The load cells were placed between two steel plates in such a manner as to equalize the load between all load cells. Figure 47 shows the calibration setup, Figure 48 shows the strain gauge arrangement and locations on the spindle, and Figure 49 shows the typical Wheatstone bridge gauge arrangement for strain cross checking.

For the C-17 tire, four load cells were arranged such that two cells measured the load on the left tire, and two cells measured the load on the right tire. This load cell arrangement allowed verification of the load distribution between the tires. Figure 50 shows the calibration results to verify that the load applied to the dual tires was evenly distributed between the two tires. Figures 51 and 52 illustrate the data used for calibrating the strain gauges attached to the carriage and to the axles. Figure 53 shows the strain gauge arrangement on the carriage. With this gauge setting and calibration procedure, it was possible to measure the load applied to the pavement as the wheel traversed the test section. Figure 54 shows the HVS-A final calibration correlated to the HVS-A load setting.

Figure 47. Calibration setup.

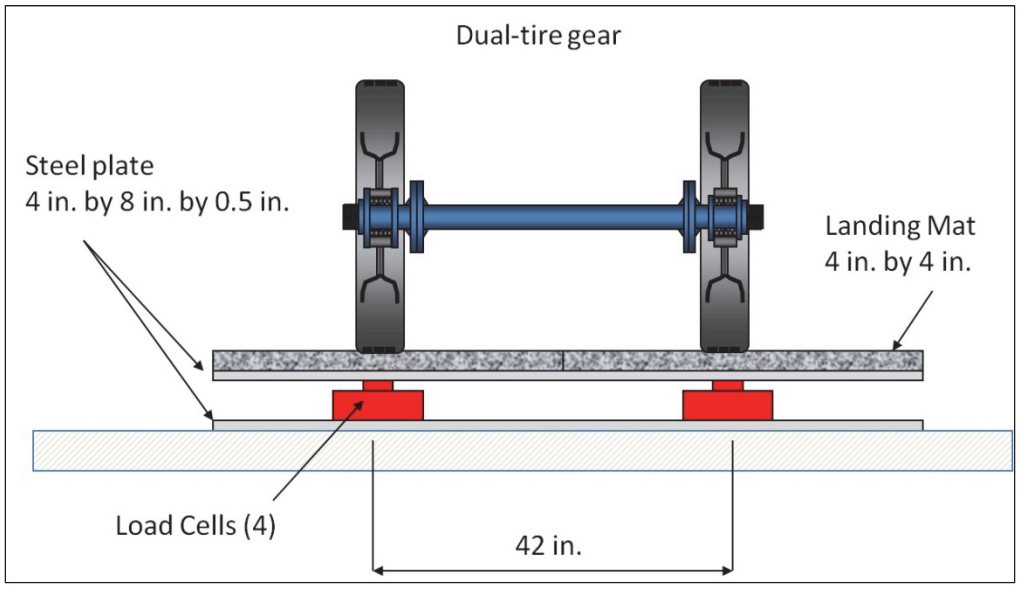

Figure 48. Schematic of strain gauge arrangement on spindle.

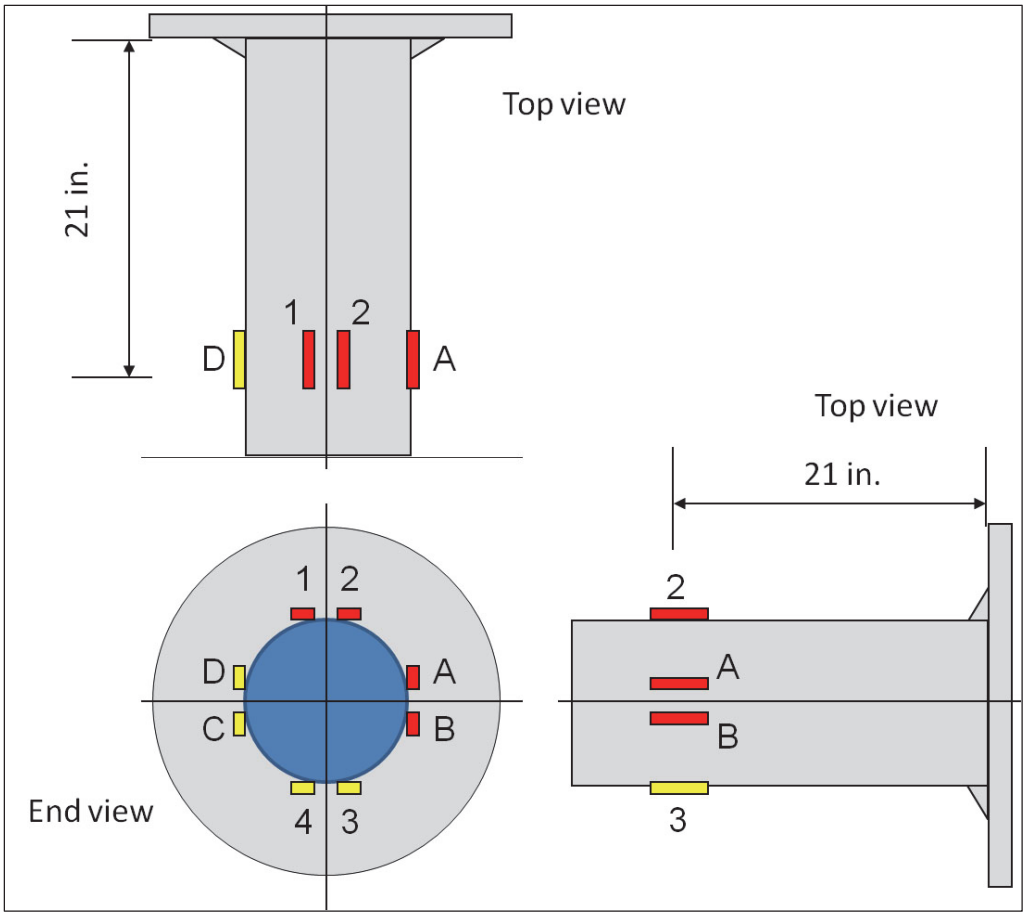

Figure 49. Gauge Wheatstone bridge.

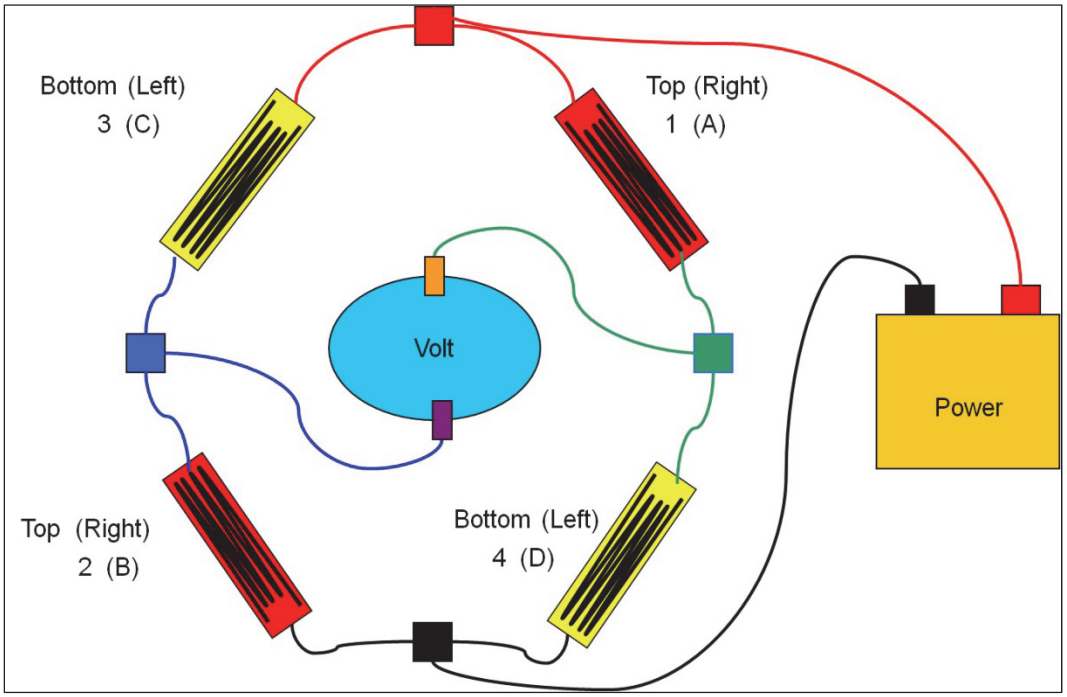

Figure 50. Load balance check between the C-17 dual tires.

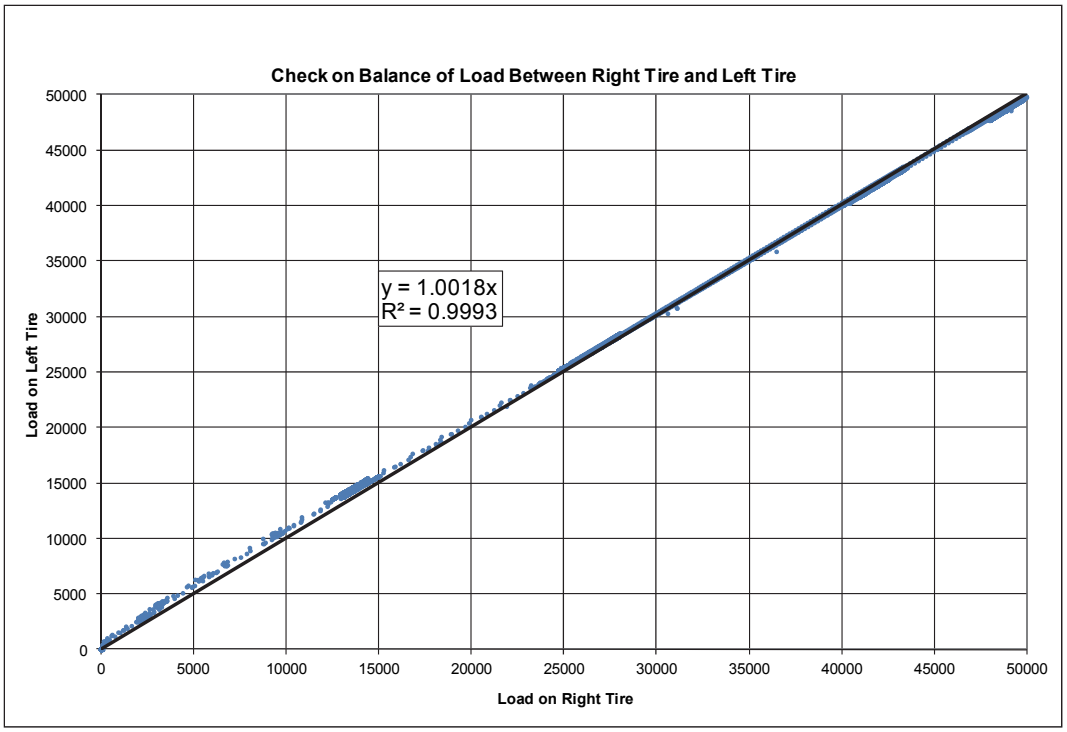

Figure 51. Load check for HVS-A carriage and axle.

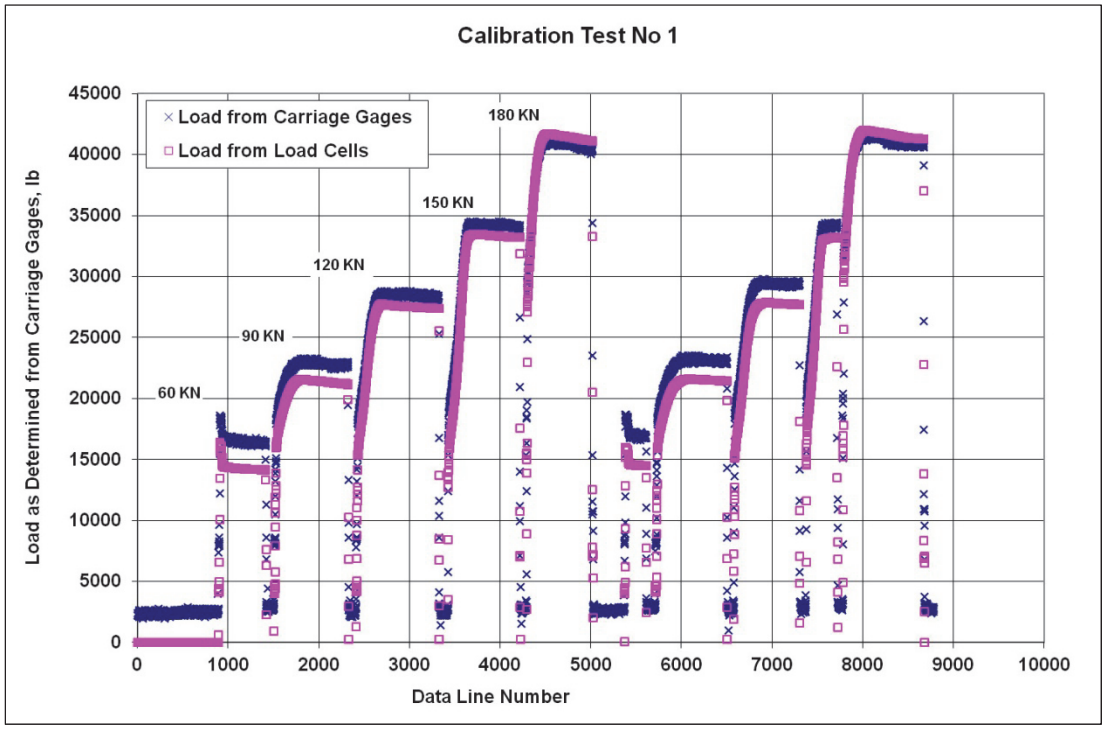

Figure 52. Carriage and axle load responses.

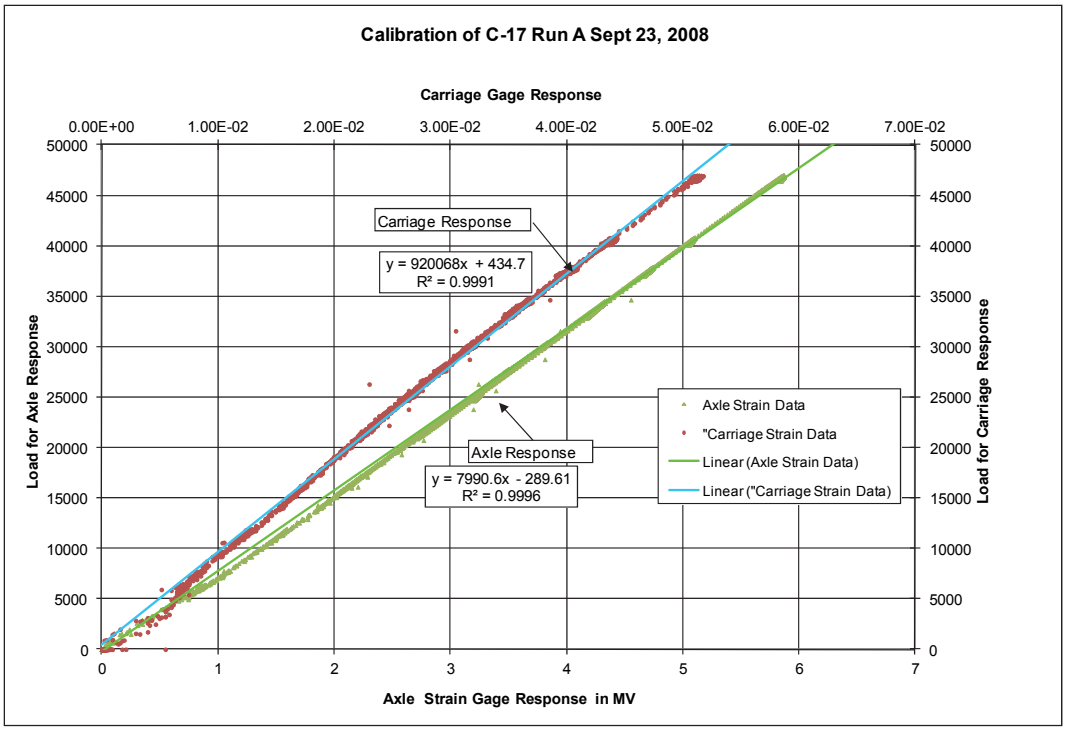

Figure 53. Carriage strain gauge arrangement.

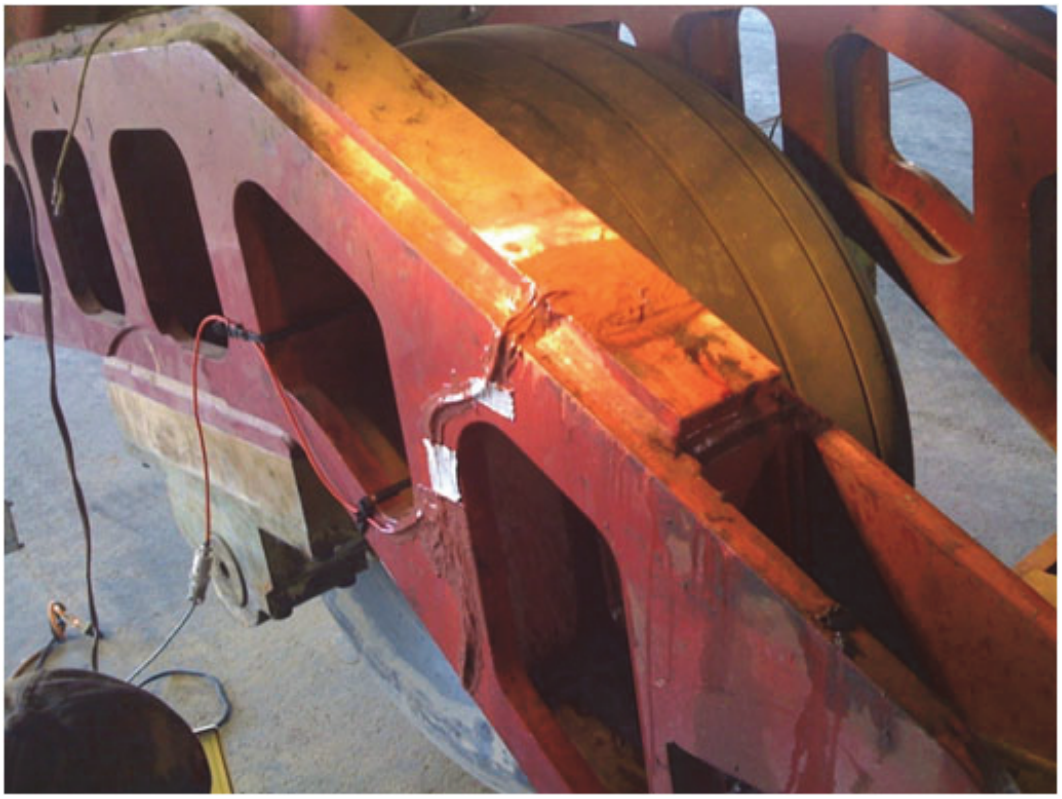

Figure 54. HVS-A load calibration.

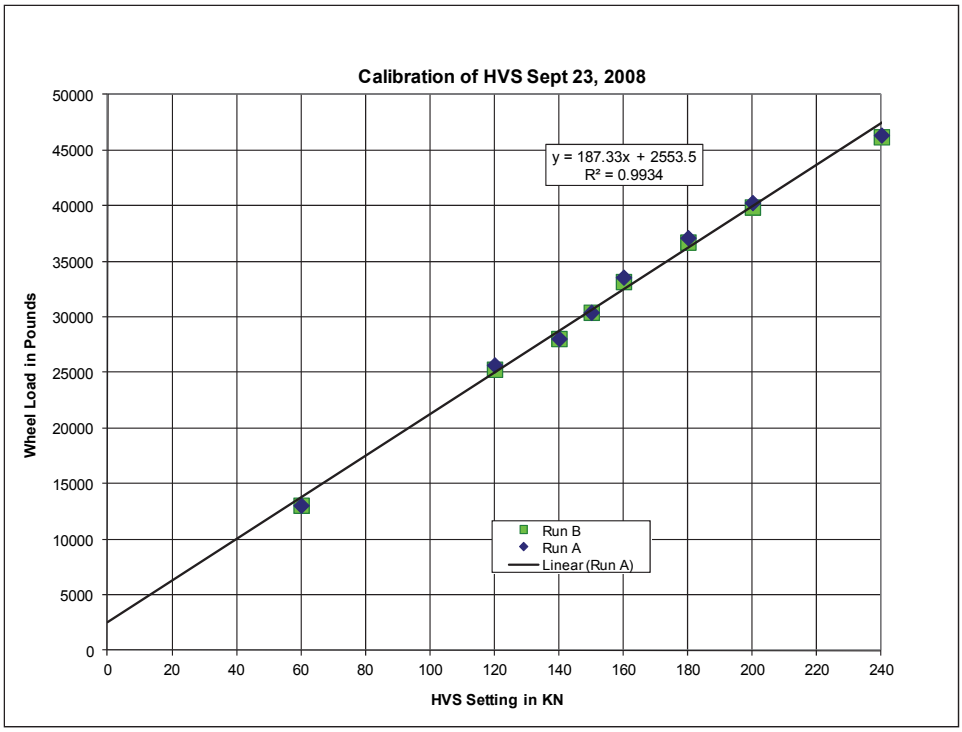

Pavement failure criteria

Historically, failure of a flexible pavement in a test section was defined by either cracking or rutting of the asphalt surface. In this study, one of the main purposes was to verify the thickness criteria with regards to rutting. Failure with regards to rutting is generally based on 1-in. rut depth. When considering the thickness criteria to protect the subgrade, this definition of rutting failure may not provide a complete assessment of the section condition; in fact, base and subbase densification instead of subgrade shear may cause surface rutting. For this reason, in order to determine a better indication of when rutting occurred in the subgrade due to shear, the rut depth was plotted as a function of the logarithm of the number of passes of the test load. Failure was then defined as the point at which the slope of the rut depth curve showed a significant increase. For almost all of the test items, the slope of the curve increased rapidly at rut depths between 1 and 2 in. This threshold point was also anticipated by cracking of the asphalt surface.

6 Behavior of Pavement Under Traffic

The behavior of the pavement under traffic was monitored through the instrumentation response and visual reports of the progressive appearance of distress. Rutting and surface profile measurements of each lane and item were obtained after a pre-set number of passes of the gear assembly. Prior to the start of the traffic testing, additional slow rolling tests were conducted on each item of Lane 1. The test item performance description is listed in chronological order.

During the section trafficking, FWD testing was performed at specified pass intervals on each test item. Appendix A includes deflections measured at each pass interval.

Trafficking over each lane item was conducted during different periods throughout the year. Figure 55 shows the pavement temperature recordings during traffic testing.

Figure 55. Pavement temperature recording during traffic.

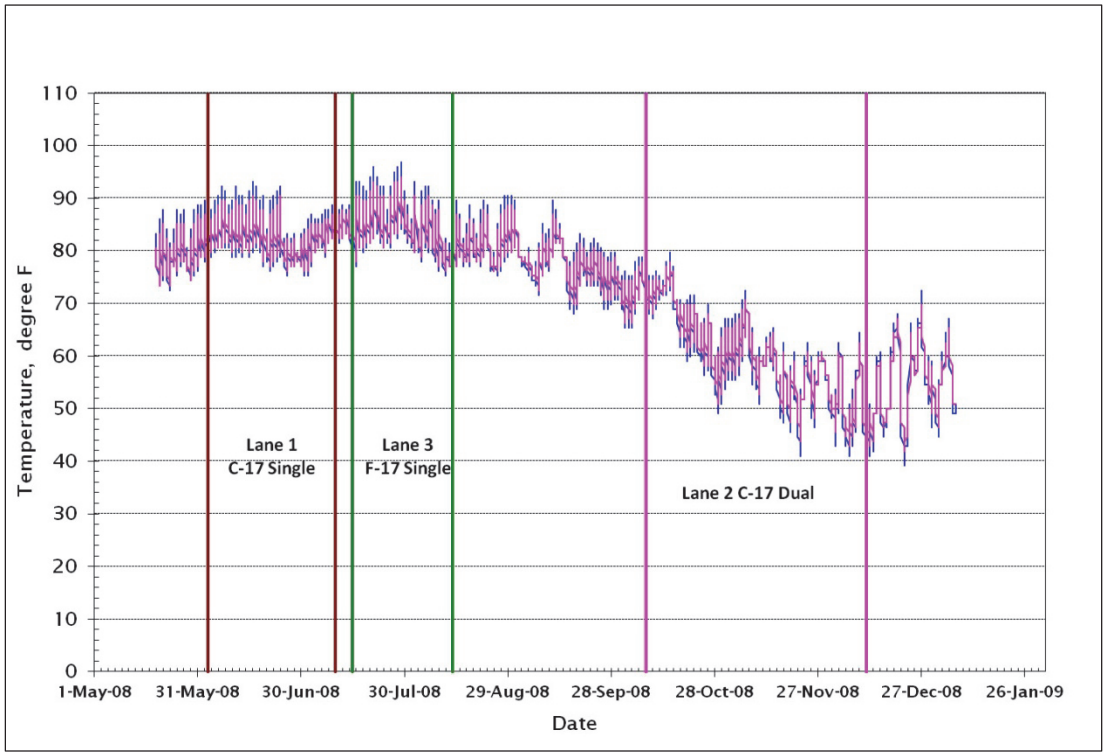

Pre-Testing sequence

A series of load tests involving all of the installed instrumentation was conducted at the beginning of trafficking, at various traffic intervals, and at the end of trafficking. The tests were given the descriptive names of Static Test, Short Roll Test, and Long Roll Test. The Static Test involved placing the tire in the raised position over the test point, applying 1/3 the test load, and letting the loaded tire remain on the pavement surface until the load was completely stable. The load was then released, and the tire was raised to the starting position. The loading process was repeated for 2/3 of the test load and for the full test load. The Static Test was repeated for the surface strain gauges and for the location of each subgrade pressure cell. After completion of the Static tests, the Short Roll Test, consisting of placing the carriage at the south end of the test item and making four passes of the tire along the center tire lane of the traffic pattern, with all gauges being recorded, took place. After completion of the Short Roll Test, the Long Roll Test was conducted. The Long Roll Test consisted of two passes, one from south to north then back to the south end along each wheel path in the traffic pattern. During this test, the carriage was in automatic control; thus, speed would be at the normal trafficking speed of about 5 mph. During the Long Roll testing, all instrumentation data were recorded with the exception of the surface deflection gauges. The description and discussion of the pre-traffic rolling tests and the analysis of the surface strain gauge data are not part of this report.

Testing sequence

After pre-testing, trafficking on the test-section lanes started. The following section includes the description of each lane item performance – the presentation order is chronological, based on the time of testing.

Lane 1 Item 4

Lane 1 Item 4 was trafficked with a C-17 single tire with a tire pressure of 142 psi and loaded to 45,000 lb. The traffic pattern was shown in Figure 44 and included 40 passes. Traffic testing on this item started 3 Jun 2008. A full set of data was obtained after application of one traffic pattern. The data included transverse and longitudinal profiles; rut depths at station 10, 20, and 30; static load tests at the EPC and strain gauge locations; and surface deflections. The average rut depth after 40 passes was approximately 0.167 in. Additional traffic patterns were applied until 12 Jun 2008, recording data at specified intervals. Table 11 summarizes the traffic data and pavement performance of the Lane 1 Item 4.

The first crack on the asphalt surface appeared after a total of 1,720 passes; the crack was less than 1/16 in. wide. After 4,143 passes, the crack had not propagated any further and had not gotten any wider. After 6,456 passes, new cracks had appeared on the surface, and the very first crack had propagated. On June 13, due to an HVS-A malfunction in lifting the tire for repositioning, a zigzag traffic pattern was applied in order to complete traffic testing on the lane item and to limit testing delays (data not included in Table 11). The P/C ratio for this pattern was 2.412. Since the applied passes were already in the order of the thousands, the change in the traffic pattern did not seem to have any influence on the permanent deformation (rutting) of the pavement section. Figure 56 summarizes the rutting development as a function of the number of total passes applied to Lane 1 Item 4.

Table 11. Lane 1 Item 4 cumulative passes and rut depth.

Month/Day (2008)	Cumulative Number of Passes	Average Rut Depth (in.)
06/03	40	0.167
06/04	400	0.563
06/04	1,320	1.000
06/05	2,240	1.229
06/09	3,003	1.417
06/10	4,000	1.417
06/11	5,600	1.625
06/12	7,545	1.750
06/12	10,000	1.938

Figure 56. Rutting development on Lane 1 Item 4.

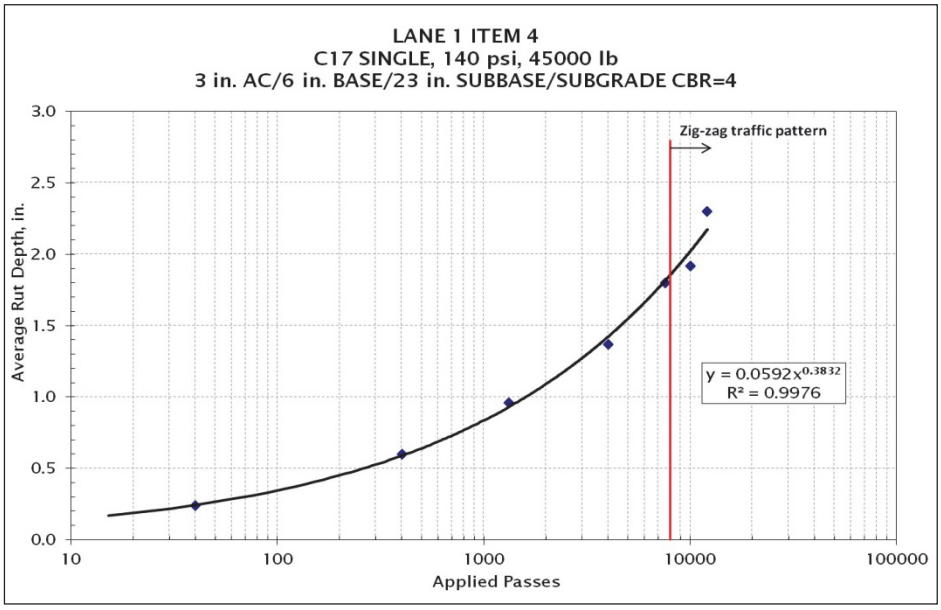

Lane 1 Item 3

Testing of Lane 1 Item 3 started on 20 Jun2008. The C-17 single tire with pressure of 142 psi and loaded to 45,000 lb was applied to the pavement. After the initial 40 passes, there was already some rutting. The maximum rutting depth was 0.375 in. After an additional 80 passes, the maximum rut depth increased to 0.563 in.; and after 160 passes, a maximum rut depth of 0.813 in. was reached. After a total of 2,000 passes, the maximum rutting was 3 in., although the section showed an average rut depth of 2.646 in. Table 12 summarizes the traffic data and pavement performance of Lane 1 Item 3. Cracking appeared on the pavement surface after 1,500 to 2,000 total passes during the last day of testing. Figure 57 includes the rutting development as a function of the number of passes.

Table 12. Lane 1 Item 3 cumulative passes and rut depth.

Month/Day (2008)	Cumulative Number of Passes	Average Rut Depth (in.)
06/20	40	0.313
06/20	80	0.479
06/20	160	0.646
06/21	400	1.167
06/23	800	1.667
06/24	1,000	1.854
06/24	1,339	1.854
06/25	2,000	2.646

Figure 57. Rutting development on Lane 1 Item 3.

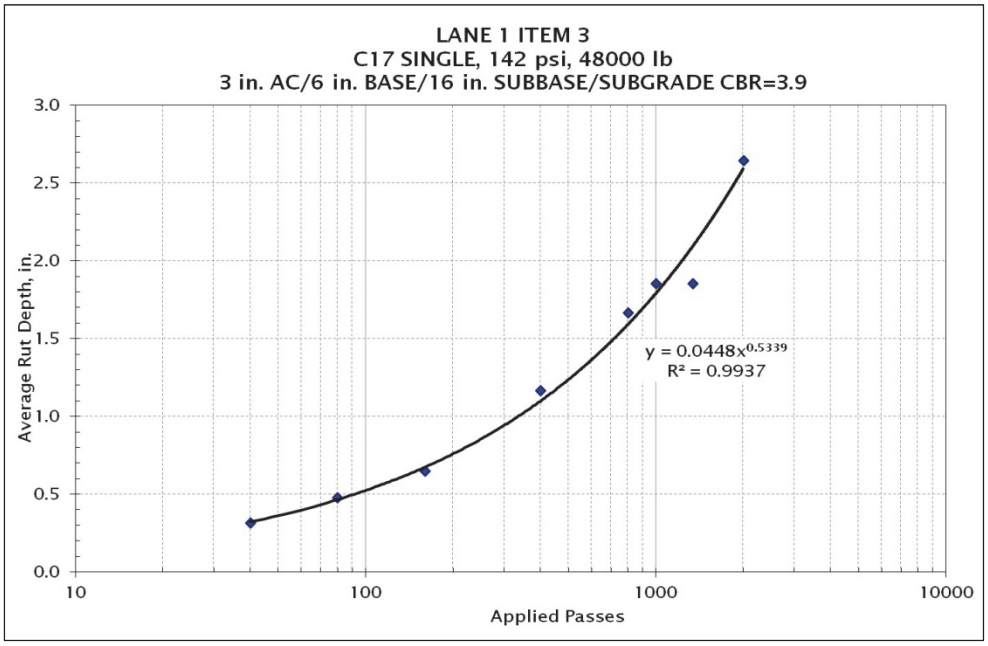

Lane 1 Item 2

Testing of Lane 1 Item 2 started 1 Jul2008. The C-17 single tire with a tire pressure of 142 psi and loaded to 45,000 lb was applied to the pavement. After the completion of 3,960 passes, the rut depth at the center of the traffic area was 1.25 in. There was no visible cracking. After 8,354 passes, a crack had formed along the southeast edge of the traffic lane outside the wheel path. Additional hairline cracks had appeared after 12,000 passes. Table 13 and Figure 58 show the rutting data as a function of the number of passes up to 8,473 passes.

Table 13. Lane 1 Item 2 cumulative passes and rut depth.

Month/Day (2008)	Cumulative Number of Passes	Average Rut Depth (in.)
07/01	120	0.104
07/01	360	0.229
07/01	1,200	0.500
07/01	3,960	1.146
07/03	8,473	1.333

Figure 58. Rutting development on Lane 1 Item 2.

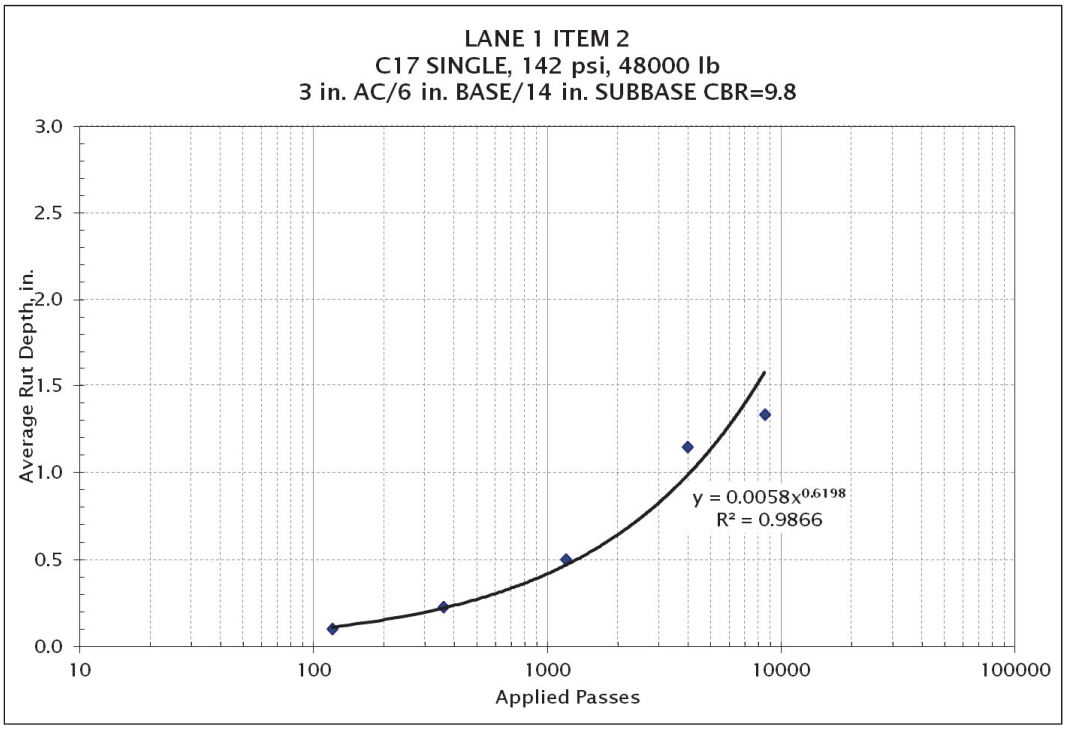

Lane 1 Item 1

Testing of Lane 1 Item 1 started 11 Jul 2008. The C-17 single tire with tire pressure set at 142 psi and loaded to 45,000 lb was applied to the pavement. After the completion of 1,200 passes, the rut depth at the center of the area was 1.75 in. There were no visible cracks. Table 14 and Figure 59 show the rutting data as a function of the number of passes.

Table 14. Lane 1 Item 1 cumulative passes and rut depth.

Month/Day (2008)	Cumulative Number of Passes	Average Rut Depth (in.)
07/11	120	0.521
07/11	360	0.958
07/11	1,200	1.750

Figure 59. Rutting development on Lane 1 Item 1

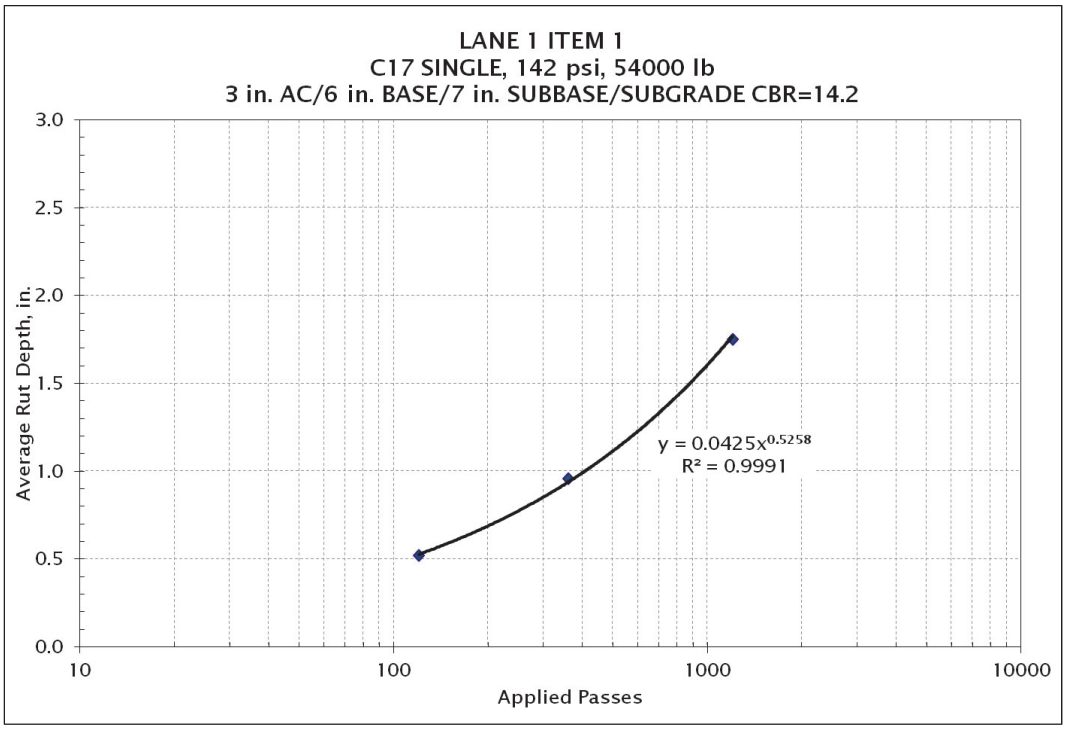

Lane 3 Item 1

Testing of Lane 3 Item 1 started 15 Jul 2008. The F-15 single tire with a tire pressure set at 325 psi and loaded to 35,000 lb was applied to the pavement. After the completion of 264 passes, the rut depth at the center of the trafficked area was 1.0 in. There was visible cracking in the center of the test item. With the addition of 264 more passes for a total of

528 passes, multiple longitudinal cracks had developed throughout the test item. The average rut depth was 1.5 in. and increased to 1.7 in. after 792 passes. Traffic was concluded after 1,056 passes with the pavement having an average rut depth of 2.146 in. Table 15 and Figure 60 show the rutting data as a function of the number of passes.

Table 15. Lane 3 Item 1 cumulative passes and rut depth.

Month/Day (2008)	Cumulative Number of Passes	Average Rut Depth (in.)
07/15	5	0.000
07/16	264	0.771
07/16	528	1.292
07/16	792	1.708
07/16	1,056	2.146

Figure 60. Rutting development on Lane 3 Item 1.

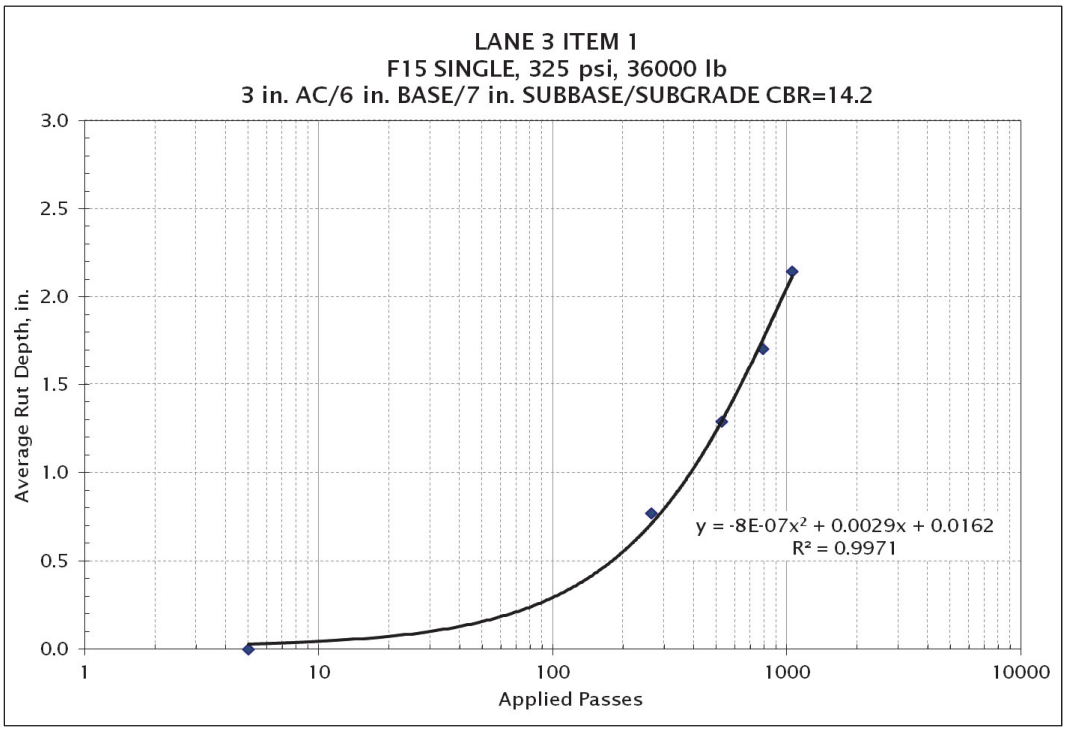

Lane 3 Item 3

Testing of Lane 3 Item 3 started 22 Jul 2008. The F-15 single tire with a tire pressure set at 325 psi and loaded to 35,000 lb was applied to the pavement. After 264 passes, multiple cracks appeared in the asphalt surface. The total number of passes applied to this item was 390. Table 16 and Figure 61 show rutting depth in relation to the number of passes.

Table 16. Lane 3 Item 3 cumulative passes and rut depth.

Month/Day (2008)	Cumulative Number of Passes	Average Rut Depth (in.)
07/22	1	0.020
07/22	264	1.438
07/23	390	1.979

Figure 61. Rutting development on Lane 3 Item 3.

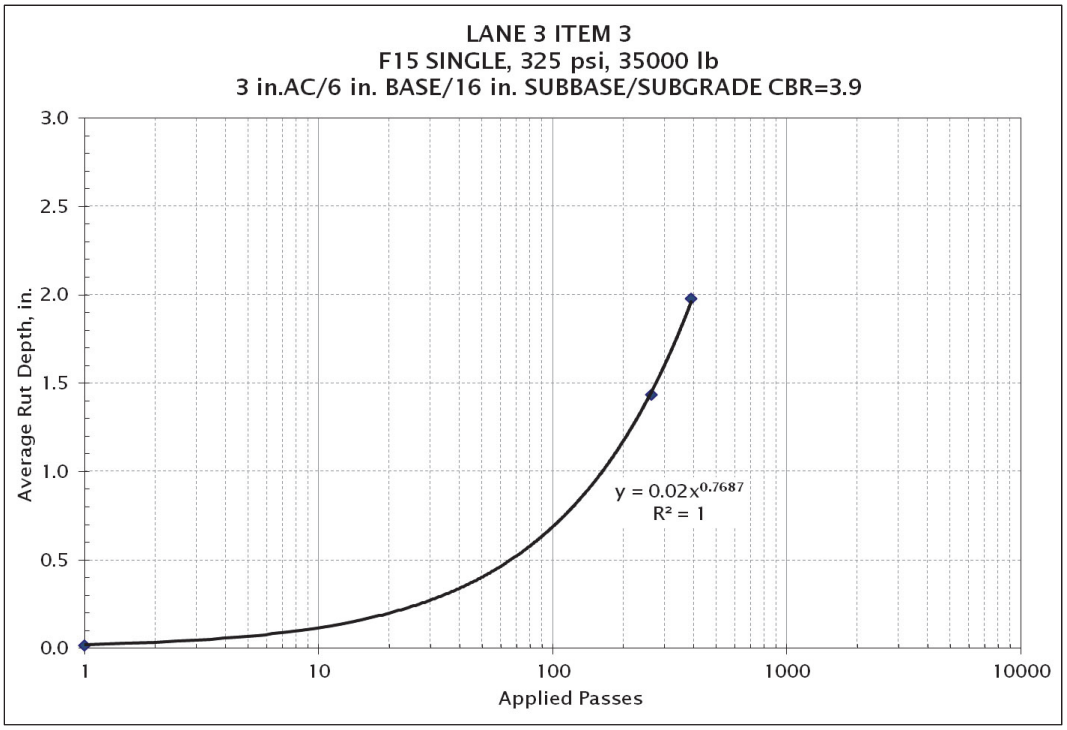

Lane 3 Item 2

Testing of Lane 3 Item 2 started 24 Jul 2008. The F-15 single tire with a tire pressure set at 325 psi was applied to the pavement. The load was reduced from 35,235-lb to 33,800 lb with the intention of increasing the expected traffic level. In addition, the initial traffic pattern was changed from 12 passes per wheel location to 6 passes per wheel location in order to better capture the initial deterioration curve. After 1,320 passes, the rut depth was 1.13 in., and few cracks had appeared on the asphalt surface. The total number of passes applied to this item was 3,350, causing an average rut depth of 1.813 in. Table 17 and Figure 62 show rutting depth in relation to the number of passes.

Table 17. Lane 3 Item 2 cumulative passes and rut depth.

Month/Day (2008)	Cumulative Number of Passes	Average Rut Depth (in.)
07/24	5	0.000
07/24	126	0.230
07/25	396	0.500
07/26	1,320	1.125
07/29	3,350	1.813

Figure 62. Rutting development on Lane 3 Item 2

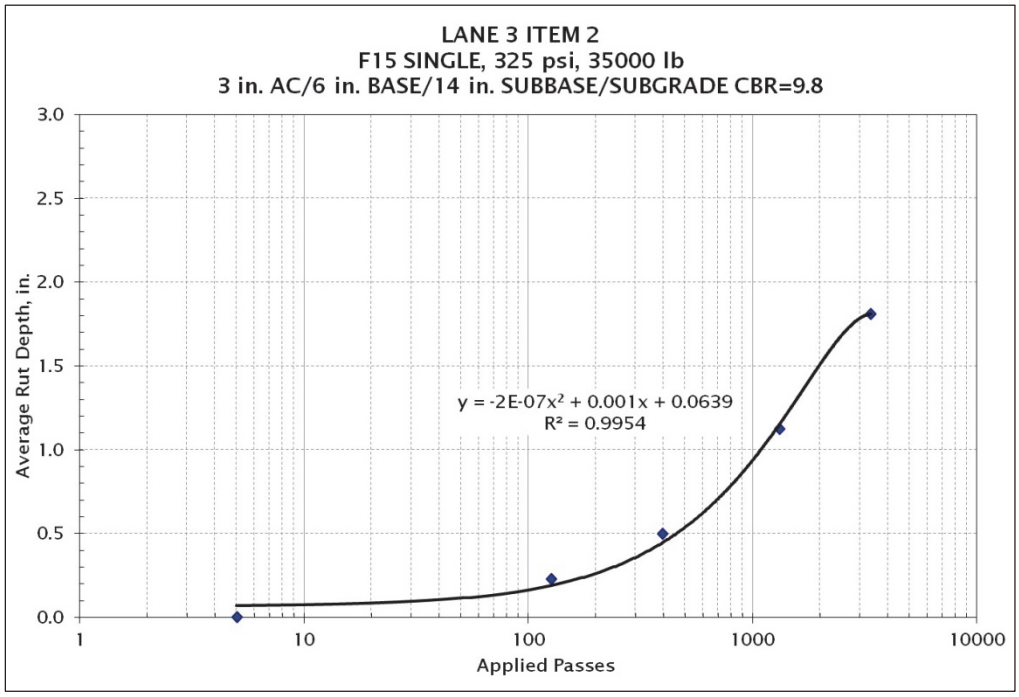

Lane 3 Item 4

Testing of Lane 3 Item 4 started 13 Aug 2008. The F-15 single tire with a tire pressure set at 325 psi and loaded to 35,235 lb was applied to this section item. After 132 passes, the rut depth was 0.354 in. The total number of passes applied to this item was 10,000, causing an average rut depth of 2.229 in. Table 18 and Figure 63 show rutting depth in relation to the number of passes.

Table 18. Lane 3 Item 4 cumulative passes and rut depth.

Month/Day (2008)	Cumulative Number of Passes	Average Rut Depth (in.)
08/13	132	0.354
08/13	1,320	1.104
08/14	10,000	2.229

Figure 63. Rutting development on Lane 3 Item 4.

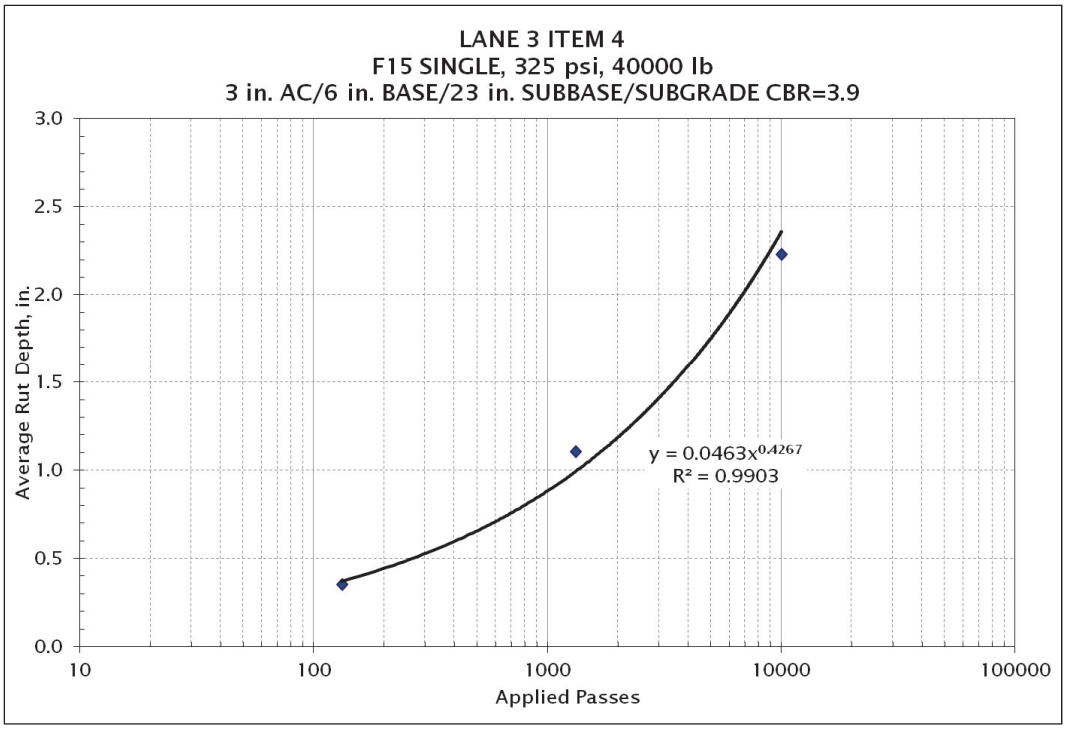

Lane 2 Item 1

Testing of Lane 2 Item 1 started 7 Oct 2008. The C-17 dual tires with a tire pressure of 142 psi and loaded to 45,000 lb per tire was applied to this section item. The rut depth after 2,640 passes was 1.021 in. On the other hand, cracking had appeared on the pavement surface after 800 passes; after 2,500 passes, cracks had progressed considerably, existing cracks had widened, and new cracks had appeared on the pavement surface. Table 19 and Figure 64 show rutting depth in relation to the number of passes.

Table 19. Lane 2 Item 1 cumulative passes and rut depth.

Month/Day (2008)	Cumulative Number of Passes	Average Rut Depth (in.)
10/07	44	0.250
10/09	80	0.229
10/10	240	0.250
10/10	800	0.646
10/14	2,640	1.021

Figure 64. Rutting development on Lane 2 Item 1.

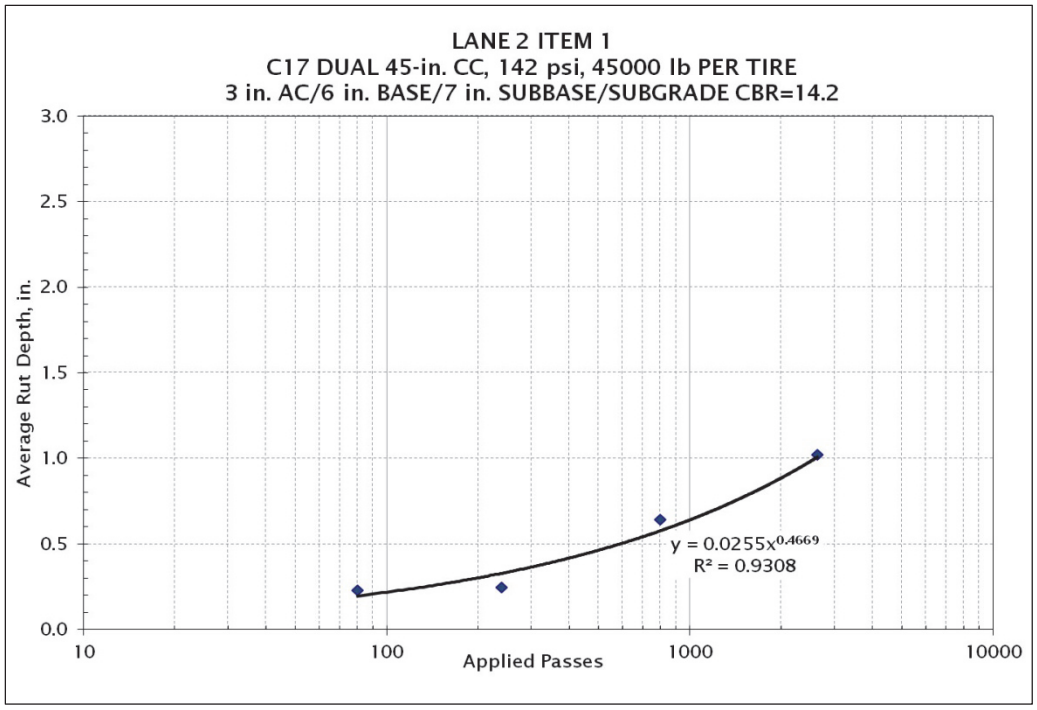

Lane 2 Item 2

Testing of Lane 2 Item 2 started 21 Oct 2008. The C-17 dual tires with a tire pressure of 142 psi and loaded to 45,000 lb per tire was applied to this section item. Only 40 passes were applied the first testing day. On 23 Oct 2008, 240 passes were completed, and the rut depth was 0.25 in. No cracks were detected. After the completion of 10,000 passes, the maximum rut depth was 1 in., and fine cracks had appeared on the pavement surface. Additional passes were applied and, at 14,600 passes, rut depth was 1.125 in. and more cracks affected the test item. Table 20 and Figure 65 show rutting depth in relation to the number of passes.

Table 20. Lane 2 Item 2 cumulative passes and rut depth.

Month/Day (2008)	Cumulative Number of Passes	Average Rut Depth (in.)
10/21	80	0.271
10/23	240	0.250
11/04	800	0.333
11/04	2,640	0.563
11/05	8,000	0.938
11/06	10,000	0.979
11/06	12,080	1.021
11/06	14,160	1.080
11/07	18,000	1.500

Figure 65. Rutting development on Lane 2 Item 2.

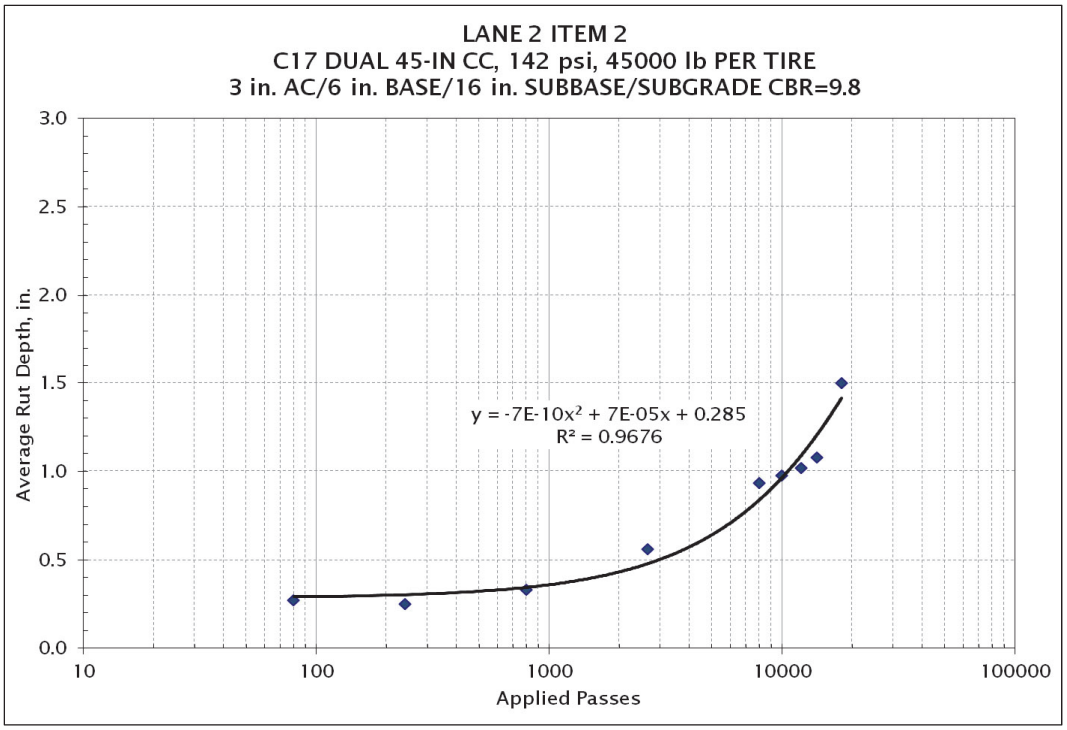

Lane 2 Item 3

Testing of Lane 2 Item 3 started 17 Nov 2008. The C-17 dual tires with a tire pressure of 142 psi and loaded to 45,000 lb per tire were applied to this section item. The first 40 passes caused rutting of 0.063 in. After 400 passes, rutting was 0.25 in., and multiple fine cracks had appeared on the pavement surface. At 1,320 passes, the section was considerably cracked; the cracks extended for the full length of the test item. The maximum rut depth was 2 in. Table 21 and Figure 66 show rutting depth in relation to the number of passes.

Table 21. Lane 2 Item 3 cumulative passes and rut depth.

Month/Day (2008)	Cumulative Number of Passes	Average Rut Depth (in.)
11/17	40	0.270
11/17	120	0.458
11/17	400	0.479
11/19	800	0.729
11/20	1,320	1.583

Figure 66. Rutting development on Lane 2 Item 3

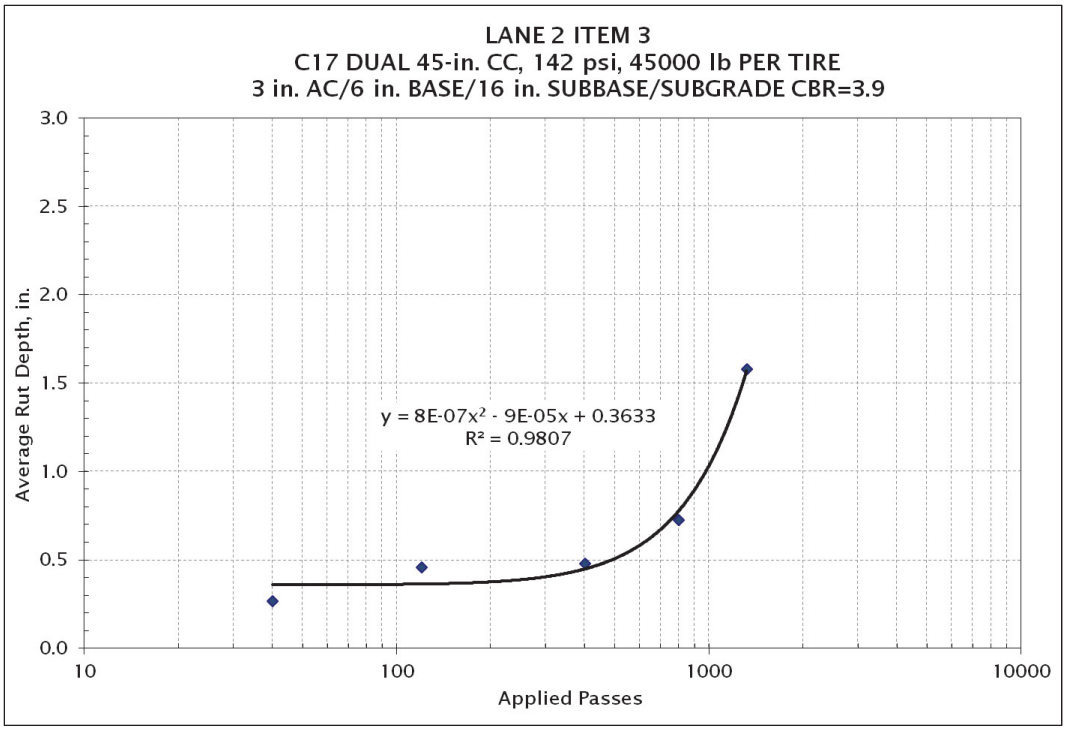

Lane 2 Item 4

Testing of Lane 2 Item 4 started 1 Dec 2008. The C-17 dual tires with a tire pressure of 142 psi and loaded to 45,000 lb per tire were applied to this section item. The first 40 passes caused rutting of 0.063 in. At 2,640 passes, the section was considerably cracked with a crack extending the full length of the test item; the maximum rut depth was 0.729 in. Traffic was stopped after 6,500 passes with an average rut depth of 1.25 in. Table 22 and Figure 67 show rutting depth in relation to the number of passes.

Table 22. Lane 2 Item 4 cumulative passes and rut depth.

Month/Day (2008)	Cumulative Number of Passes	Average Rut Depth (in.)
12/01	40	0.063
12/01	200	0.118
12/03	800	0.350
12/04	2,640	0.729
12/04	3,000	1.020
12/05	6,500	1.250

Figure 67. Rutting development on Lane 2 Item 4

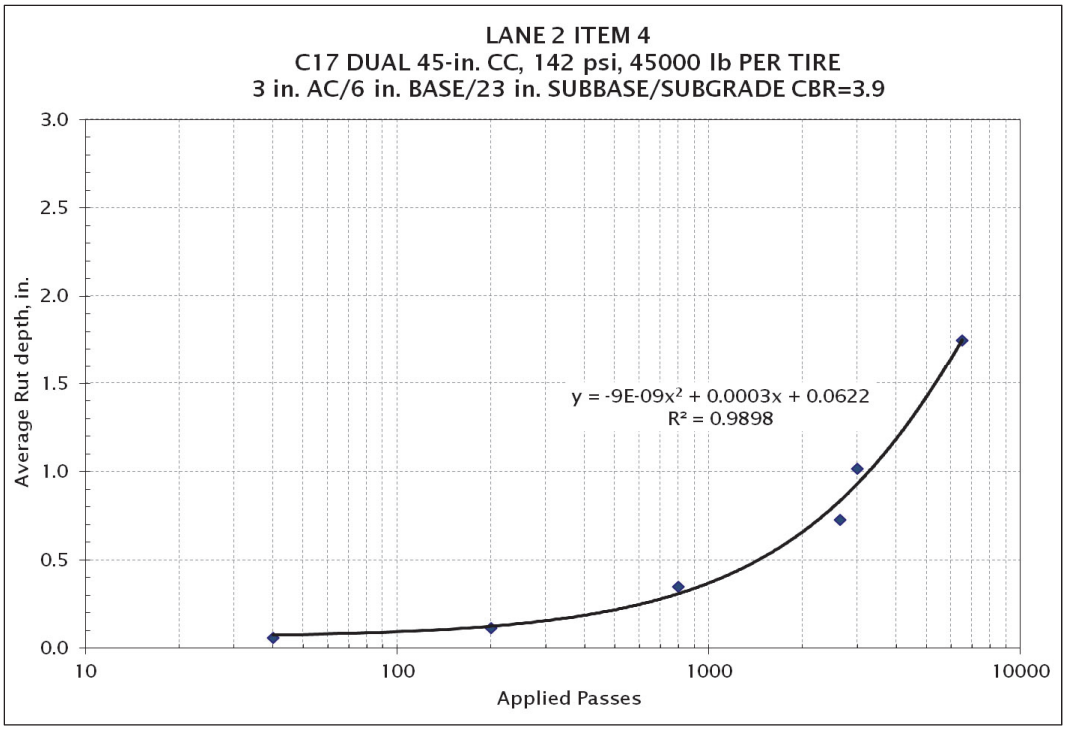

Considerations on the section performance under traffic

The test section performance under traffic can be analyzed in two ways: considering the item structure or the applied traffic. Each traffic lane included four items with different structural characteristics. Table 23 summarizes item passes to failure and average rut depth at failure.

Table 23. Summary of the passes to failure and rut depth.

Lane	Item	Number of Passes at Failure	Average Rut Depth (In.)
1	1	360	0.958
	2	1,200	0.500
	3	400	1.167
	4	4,000	1.417
2	1	2,640	1.021
	2	14,160	1.080
	3	800	0.729
	4	3,000	1.020
3	1	400	0.771
	2	1,000	0.563
	3	100	0.458
	4	1,320	0.360

Lane 1 was subjected to the traffic applied by a C-17 single tire. From the tables and charts describing the items' performances under traffic, it is possible to note that the combination of subbase thickness and subgrade CBR most likely were the controlling factors of the pavement failure. A section is considered failed when exhibiting at least 1 in. of rutting. Item 4, characterized by a subbase thickness of 23 in. and subgrade CBR of 4, failed quite late after 1,320 passes. In Item 3 the decrease in subbase thickness to 16 in. and still maintaining the subgrade CBR at 4 produced early failure after only 300 passes. The latter value was extrapolated from the rut depth measurements performed at specified pass intervals. Item 2 showed better performance than Items 3 and 4, failing at about 3,100 passes (extrapolated value). The structure of Item 2 included the subbase thickness of 13 in. and subgrade CBR of 10. The failure of Item 1 was quite immediate after only 360 passes. Item 1 had a subbase thickness of 6 in. and subgrade CBR of 15. For this item, the increased subgrade CBR, to handle the decrease in the subgrade thickness to 6 in., did not assure section performance. The thinner subbase was unable to protect the subgrade from shearing. By comparing the CBR data of Items 4, 3, and 2, the increase in subgrade CBR to 10 in Item 2 was able to compensate for the decrease in subbase thickness to 13 in.

Lane 2 was trafficked with a C-17 dual-tire gear. As in the test items included in Lane 1, Item 2 had the best performance: 1 in. of rut depth was reached after 12,080 passes. The worst performer was Item 3. The relationship between subbase thickness and subgrade CBR is also evident in this case when the traffic load is imposed through a dual-tire gear. For each Lane 2 item, the number of passes was higher than the number of passes to failure for the items in Lane 1. This aspect may be a result of the dual-tire load distribution throughout the pavement structure.

Lane 3 was trafficked with an F-15 single tire with an inflation pressure of 325 psi. In this case, Item 4 had the best performance, reaching failure after 1,320 passes. Item 4 was characterized by a subbase thickness of 23 in. and subgrade CBR of 4. The second in performance was Item 2 (as in the other two testing lanes) with failure at 1,000 passes (value extrapolated from intermediate performance assessments at specified pass intervals). Items 3 and 1 had early failure at 100 and 400 passes, respectively. The influence of the pavement structure is evident, as it was for the other two test lanes. Also, load distribution to the pavement through a single tire rather than a dual tire (as in Lane 2) was also evident in the overall lower number of passes to failure than those measured for the items in Lane 2.

7 Summary of Findings, Conclusions, and Recommendations

Summary of findings

The findings from the traffic testing of the flexible pavement section characterized by pavement structures with different values of subgrade CBR and subbase thickness showed the following:

1. The combination of subbase thickness and subgrade CBR was the controlling factor with the highest impact on pavement failures. This was observed for each item on each traffic lane independently from the type of applied traffic.
2. Lane 1 was subjected to the traffic applied with a C-17 single tire loaded to 45,000 lb. The comparison of the CBR values of Items 2, 3, and 4 showed that the increase in subgrade CBR compensated for the decrease in subbase thickness.
3. For Item 1 in Lane 1, the failure occurred after only 360 passes. The subgrade CBR of 15 (greater than the CBR in the other Items) did not compensate for the thinner Item 1 subbase and did not assure pavement performance. The thinner subbase did not provide adequate protection and prevent the subgrade shearing.
4. Lane 2 was trafficked with a C-17 dual-tire gear loaded to 90,000 lb. For each item in Lane 2, the number of passes to failure was higher than the number of passes to failure for the items in Lane 1. This aspect may be a result of the dual-tire load distribution throughout the pavement structure.
5. The pavement items in Lane 2 also showed the influence of subbase thickness and subgrade CBR on pavement performance. The performance of thinner subbases can be compensated with an increase in subgrade CBR, thus maintaining a constant ratio applied between allowable stress, as dictated by the performance criteria being validated. None of the items in Lane 2 showed early failure as occurred for Item 1 in Lane 1.
6. Lane 3 was trafficked with an F-15 single tire. The influence of the pavement structure was evident as it was for the other two test lanes.
7. In Lane 3, the load distribution to the pavement through a single tire rather than a dual tire (as it was in Lane 2) was reflected in the overall lower number of passes to failure compared to those measured for the items in Lane 2.

8. The comparison of the pavement performance under single-tire traffic applied to Lanes 1 and 3 showed that tire pressure and contact areas have limited influence on pavement performance. Lane 1 Item 1 , trafficked with a C-17 single tire (tire pressure of 142 psi, contact area of 148 in.^{2}) failed after 360 passes; whereas, Lane 3 Item 1, trafficked with a F-15 single tire (tire pressure of 325 psi, contact area 110 in.^{2}) failed after 400 passes. Early failure occurred for Lane 3 Item 3 after only 100 passes, and early failure occurred for Lane 1 Item 3 after 400 passes.

Conclusions

Results from analyses performed on the data collected during this full-scale test help substantiate the following conclusions:

1. The pressure distribution acting at the top of the subgrade is influenced by the material strength and thickness of the entire system.
2. In contrast with the assumption of Odermark's method for which the stresses acting below a layer depend only on the stiffness of that layer (Ullidtz, 1998),

    a. The layer thickness and its confinement, characterized by the existence (and strength) of an underlying layer also have influence on the stresses acting on the layer itself.
    b. The shear strength of the subgrade, quantified by the CBR, and the subbase thickness has influence on the stress distribution acting at the top of the subgrade.

In light of these conclusions, it was possible to confirm the relationship between Fröhlich's stress concentration factor and subgrade CBR and thus validate the proposed CBR-Beta design procedure for flexible pavements. A combined analysis of the measured data and theoretical considerations representing the basis of the design procedure confirmed the theoretical hypothesis of the model. The theoretical development and data analysis of the CBR-Beta procedure are contained in the Volume 1 of the series *Reformulation of the CBR procedure* (ERDC/GSL TR-12-16, Vol. 1).

Recommendations

Based on the performance of the flexible test section constructed for this project, traffic testing with different loadings, and the analysis and evaluation of the theoretical model, it is recommended that

1. the performance and response data be further analyzed with the objective of improving the existing CBR-Beta model and flexible pavement design criteria for conditions other than those tested in this full-scale test section;
2. additional studies should be conducted to evaluate if the CBR-Beta procedure can also be implemented for road designs characterized by lighter load ranges but higher number of passes;
3. pavement structures with thicker asphalt layers should also be investigated and correlated to the results obtained from these tests;
4. pavement structures containing stabilized layers should also be investigated and correlated to the CBR-Beta procedure;
5. the influence of granular layers of different thicknesses on the resulting pressure distribution for the subgrade should be investigated;
6. additional data collected from the falling weight deflectometer, strain gauges, and multi-depth deflectometer should be analyzed with the objective of developing more advanced finite element modeling procedures.

References

Aerodrome Operations and ICAO Services Working Group. 2006. *Discussion paper No. 21*.

ASTM. (n. d.). *D6938-10 standard test method for in-place density and water content of soil and soil-aggregate by nuclear methods (shallow depth)*. American Society for Testing and Materials.

_____. (n. d.). *D1557-12 standard test methods for laboratory compaction characteristics of soil using modified effort (56,000 ft-lbf/ft³ (2,700 kN-m/m³))*.

_____. (n. d.). *D1883-07e2 standard test method for CBR (California Bearing Ratio) of laboratory-compacted soils*.

_____. (n. d.). *C568/C568M - 10 standard specification for limestone dimension stone*.

CROW. 2004. *The PCN runway strength rating and load control system*. Report D04-09. Amsterdam, the Netherlands: Information and Technology Platform for Transport, Infrastructure and Public Space.

Gonzalez, C. R., W. R. Barker, and A. Bianchini. 2012. *Reformulation of the CBR procedure*. ERDC/GSL TR-12-16, Vol 1. Vicksburg, MS: US Army Engineer Research and Development Center.

ICAO. 1983. *Aerodrome design manual*. Doc 9157-AN/901. Montreal: International Civil Aviation Organization.

Kondner, K. L. 1963. Hyperbolic stress-strain response: Cohesive soils. *J. of the Soil Mechanics and Foundation, ASCE* 89(SM 1):115-143.

Ledbetter, R. H., J. L. Rice, H. H. Ulery, F. W. Kearney, J. B. Gambill, and J. W. Hall. 1971. *Multiple-wheel heavy gear load pavement tests*. Technical Report S-71-17. Vicksburg, MS: US Army Engineer Waterways Experiment Station.

Middlebrooks, T. A., and G. E. Bertram. 1950. Adaptation to the Design of Airfield Pavements. *Transactions, ASCE* 468-470.

Ullidtz, P. 1998. *Modeling Flexible Pavement Response and Performance*. Denmark: Polytenisk Forlag.

USACE. 2012. Hot-Mix Asphalt Airfield Paving. *Unified Facilities Guide Specifications* 32(12):15.13.

Waterways Experiment Station. 1971. *Multiple-wheel heavy gear load pavement tests*. Technical Report S-71-17. Vicksburg, MS: US Army Corps of Engineers.

Appendix A

Appendix A contains the data of the field tests executed during construction and traffic. The tests include CBR and DCP tests and FWD measurements executed on the subgrade, subbase, and base layers during construction. For each item and testing lane, the appendix also includes deflections measured at specific pass intervals during the pavement performance assessment.

The information for this appendix can be obtained by contacting the ERDC Library at 601-634-2355 or erdclibrary@usace.army.mil.

REPORT DOCUMENTATION PAGE

Form Approved
OMB No. 0704-0188

1. REPORT DATE *(DD-MM-YYYY)*	2. REPORT TYPE	3. DATES COVERED *(From - To)*
December 2013	Report 2	

4. TITLE AND SUBTITLE

Reformulation of the CBR Procedure; Volume II: Design, Construction, and Behavior Under Traffic of the Pavement Test Sections

5a. CONTRACT NUMBER

5b. GRANT NUMBER

5c. PROGRAM ELEMENT NUMBER

6. AUTHOR(S)

Carlos R. Gonzalez, Walter R. Barker, and Alessandra Bianchini

5d. PROJECT NUMBER

5e. TASK NUMBER

5f. WORK UNIT NUMBER

7. PERFORMING ORGANIZATION NAME(S) AND ADDRESS(ES)

Geotechnical and Structures Laboratory
US Army Engineer Research and Development Center
3909 Halls Ferry Road
Vicksburg, MS 39180-6199

8. PERFORMING ORGANIZATION REPORT NUMBER

ERDC/GSL TR-12-16

9. SPONSORING / MONITORING AGENCY NAME(S) AND ADDRESS(ES)

Headquarters, US Army Corps of Engineers
Washington, DC 20314-1000

10. SPONSOR/MONITOR'S ACRONYM(S)

HQ-USACE

11. SPONSOR/MONITOR'S REPORT NUMBER(S)

12. DISTRIBUTION / AVAILABILITY STATEMENT

Approved for public release; distribution is unlimited.

13. SUPPLEMENTARY NOTES

14. ABSTRACT

The California Bearing Ratio (CBR) procedure has been the principal method used for design of flexible pavements for both military roads and airfields since its development in the 1940s. In recent years, as the use of analytical models, such as the layered elastic and finite element models, became accepted for pavement design, the CBR design procedure was criticized as being empirical, overly simplistic, and outdated. A major criticism of the procedure was the use of a correction factor (Alpha factor) as a thickness adjustment for traffic volume. The objectives of this research were to reformulate the CBR-Alpha procedure so that design would be based on a more mechanistic methodology and to develop performance criteria for use with the reformulation. With these purposes in mind, this report details the developmental steps of the reformulation, starting with the original CBR-Alpha procedure and ending with a new procedure based on Fröhlich's theory for stress distribution. The reformulation was verified through review of historical test data and full-scale traffic tests and analyses of an actual airfield pavement failure. The reformulation of the procedure resulted in the elimination of both the equivalent single-wheel load concept and the Alpha factor.

15. SUBJECT TERMS

Full-scale test section
Accelerated testing
CBR-Beta procedure validation
Flexible pavement construction
Pavement instrumentation
Strain gauges recording
Earth pressure cells recording

16. SECURITY CLASSIFICATION OF:			17. LIMITATION OF ABSTRACT	18. NUMBER OF PAGES	19a. NAME OF RESPONSIBLE PERSON A. Bianchini
a. REPORT	b. ABSTRACT	c. THIS PAGE			19b. TELEPHONE NUMBER *(include area code)*
Unclassified	Unclassified	Unclassified		84	